Master of Science

낮은 SLL과 넓은 대역폭을 위한 비균일 간격 및 급전 밀리미터파 마이크로스트립 안테나 어레이

Non-Uniformly Excited and Spaced Millimeter Wave Microstrip Antenna Array for Low SLL with Broad Bandwidth

The Graduate School

of the University of Ulsan

School of Electrical Engineering

Md. Nazim Uddin

Non-Uniformly Excited and Spaced Millimeter Wave Microstrip Antenna Array for Low SLL with Broad Bandwidth

Supervisor: Prof.Sangjo Choi

A Master's Thesis

Submitted to
the Graduate School of the University of Ulsan
in partial fulfillment of the requirements
for the degree of

Master of Science
by

Md. Nazim Uddin

School of Electrical Engineering
Ulsan, Republic of Korea

February 2021

Non-Uniformly Excited and Spaced Millimeter Wave Microstrip Antenna Array for Low SLL with Broad Bandwidth

This certifies that the Master's Thesis

of Md. Nazim Uddin is approved.

.....

Committee Chair, Prof. Hyung-Yun Kong

.....

Committee Member, Prof. Jiho Song

.....

Committee Member, Prof. Sangjo Choi

Department of Electrical Engineering

Ulsan, Republic of Korea

February, 2021

ACKNOWLEDGEMENT

All praise and thanks belong to almighty ALLAH (SWT) who is the Lord of the universe.

I would like to express my sincere gratitude to my advisor Prof. Sangjo Choi of the School of Electrical Engineering at the University of Ulsan for his supervision, advice, continuous support, and constant encouragement throughout my M.Sc. research. His patience, motivation, immense knowledge, and continuous guidance helped to conduct my research and writing of this thesis. Besides my advisors, I am gratefully indebted to my other thesis committee members: Prof. Hyung-Yun Kong**,** Prof. Jiho Song**,** for their efforts to review my thesis, insightful comments, and suggestions.

I would like to thank my lab mates Kdm Raziul Islam, Nasim Al Islam, Md Khoirul Anam, and Sang Min, in the Electromagnetics System and Physics Lab for their friendship and support. I am very much grateful to the University of Ulsan for giving me this opportunity and financial support. My special thanks go to Brain Korea 21Plus Program for its contribution and financial support during my study.

I would like to express my heartiest thanks to Surajit Chakraborty, Sheikh Mominul Hoque, Md Hasan Turabee, Md Rasel Islam, Md Jashim Uddin Shehab, Md Maruf Mridha, Md Junayed Hasan, Walid Amir, Rafia Nishat Toma, and Md Mayen Uddin for their love and support. In Ulsan, we shared countless memories that I will never forget.

Finally, I am ever grateful to my parents Md Belayet Hossain and Nasima Akhter for raising me with constant hardship and helping me to achieve all that I have in my life. I would like to acknowledge and thanks my younger brothers Md Nasir Uddin, Md Naim Uddin, and Md Nahid Uddin with whom I shared my childhood. I am ever grateful to my wife Jannatul Mawa for her support and all the sacrifices, she has made, for my achievement. I would like to acknowledge my lovely daughter Nusaiba Mahnisa Eshal, her birth has been a great influence and gave me inspiration for my higher study. At last, I want to dedicate my thesis to all of my family members who are the strength of my whole life.

Md Nazim Uddin
February, 2021
University of Ulsan

ABSTRACT

In the first part of my thesis, I demonstrate theoretical backgrounds of the microstrip antenna with parasitic patches, corporate feeding, array factor, and antenna radiation pattern and reviewed conventional methods to reduce side lobe level (SLL). The SLL reduction is necessary to reduce noise and cochannel interference in wireless communication. Usually, the SLL reduction of the microstrip antenna array can be realized by the tapering of the microstrip lines or radiating elements to feed the corresponding antenna elements with non-uniform power distribution. This tapering technique results in numerous tapered branches which eventually increase the cross-polarization of the array. In contrast, a systematic way can be employed to realize the non-uniform distribution of power by using the different levels of power split in the junction of the power divider. This method can eliminate the necessity to taper the transmission line or radiating elements. In addition to the non-uniform power distribution, recently, the spacing between the antenna elements was controlled in a non-uniform fashion to reduce SLL and the related examples are overviewed.

In the second part of my thesis, we designed a non-uniformly powered and spaced corporate feeding network to feed a 12-element parasitic patch-integrated microstrip antenna array for SLL reduction at 28 GHz in the millimeter-wave band. In the feeding network, we arranged two one-to-six-way power dividers from the opposite sides and two opposite input ports were fed 180° out-of-phase. This feeding technique demonstrated high isolation and lower mutual coupling between the adjacent antenna elements. The non-uniform power distribution was realized by using the different levels of power split in the junction of the power divider, whereas non-uniform spacing for the lowest SLL was determined using the analytical array factor. Due to the consideration of the coupling effect of the parasitic patch, the non-uniform spacing was further optimized using full-wave simulations. To verify the SLL reduction effect from the non-uniform spacing in the array, we designed two non-uniformly excited antenna arrays with uniform half-wavelength spacing and non-uniform spacing. To feed all of the antenna elements with identical electrical phase, we optimized the power split junction of both antenna arrays. Besides, non-uniform spacing introduces higher phase mismatch compared to uniform spacing, to compensate for this we introduced a meander line in the power divider section of the non-uniform spaced array. We fabricated and measured both antenna arrays, where the non-uniformly powered and spaced patch antenna array demonstrated a nearly 16.56 dBi boresight gain and −17.27 dB SLL, which is nearly 2 dB lower than the uniformly spaced counterpart. For future implementation, beamforming performance for the uniform and the non-uniform spaced array was also analyzed. Finally, we expect that the non-uniformly powered and spaced high gain patch antenna array with a low SLL will be suitable for millimeter-wave communication application.

TABLE OF CONTENTS

ACKNOWLEDGEMENT **1**

ABSTRACT **2**

TABLE OF CONTENTS **3**

LIST OF FIGURES **5**

LIST OF TABLES **7**

CHAPTER 01: INTRODUCTION **8**

1.1 Motivation and goal **8**

1.2 Thesis Organization **9**

CHAPTER 02: ANTENNA AND ANTENNA PARAMETERS **10**

2.1 The Microstrip Patch Antenna 10

2.2 The Parasitic Patch Antenna 13

2.3 The Corporate (Parallel) Feeding 16

2.4 Antenna Parameters 18

2.4.1 Radiation Pattern 18

2.4.2 Beamwidth 18

2.4.3 Directivity 18

2.4.4 Antenna Gain 19

2.4.5 Efficiency 19

2.4.6 S-Parameters (Reflection Coefficient) and Bandwidth 20

2.4.7 VSWR 20

2.5 Antenna Array and Array Factor 20

CHAPTER 03: LITERATURE REVIEW FOR ARRAY WITH LOWER SIDE LOBE LEVEL **23**

3.1 SLL Reduction Technique 23

3.1.1 Binomial Distribution 23

3.1.2 Chebyshev Distribution 24

3.2 Radiating Elements Tapering 26

3.3 Transmission Line Tapering 27

3.4 Tapering by Number of Power Level 28

3.5 Non-Uniform Spacing for SLL Reduction 29

3.6 Requirement of Millimeter-Wave Antenna 29
CHAPTER 04: NON-UNIFORMLY POWERED AND SPACED CORPORATE FEEDING ANTENNA ARRAY **30**
4.1 Introduction 30
4.2 Design and Optimization of Antenna Array 31
4.2.1 Design of Single Patch with Parasitic 31
4.2.2 Effect of Non-Uniform Spacing and Excitation 32
4.2.3 Design of Non-Uniformly Power and Uniformly Spaced Antenna Array 33
4.2.3.1 Design of Power Divider 33
4.2.3.2 Phase Correction of Power Divider 35
4.2.3.3 Patch Integration with Power Divider 36
4.2.4 Design of Non-Uniformly Power and Non-Uniformly Spaced Antenna Array 36
4.2.4.1 Design of Power Divider and Phase Correction 37
4.2.4.2 Patch Integration with Power Divider 39
4.3 Fabrication and Measurement 39
4.4 Discussion 42
CHAPTER 5: CONCLUSIONS AND FUTURE WORKS **44**
5.1 Conclusion 44
5.2 Suggestions for future works 44
5.2.1 Uniform Spaced Array Beam forming 44
5.2.2 Non-Uniform Spaced Array Beam forming 47
5.2.3 Discussion About Beam forming Array 49
References 51

LIST OF FIGURES

Figure 2.1	Microstrip antenna and corresponding coordinate system	11
Figure 2.2	Inset feed micro-strip antenna	12
Figure 2.3	Co-planar four microstrip parasitic elements coupled via radiating and non-radiating edges a) antenna configuration b) VSWR plot presented in reference	14
Figure 2.4	Stack microstrip Patch	15
Figure 2.5	Corporate feed a) Realization by tapered line b) using the quarter wave transformer	17
Figure 2.6	Corporate feed five element dipole array (mutual coupling considered inside the dotted box)	17
Figure 2.7	Radiation pattern and Beamwidth of antenna	19
Figure 2.8	A Planar Antenna Array	21
Figure 2.9	An N-element antenna array along x axis	21
Figure 3.1	Array (a) identical elements (b) tapered patch width and (c) tapered patch current distribution [31]	26
Figure 3.2	Different width Rectangular array with parallel feeding [33]	26
Figure 3.3	Configurations of array. a) Patch width-tapering; b) line-width tapering [35]	27
Figure 3.4	Configuration of SIW unequal 8-way power divider [38]	27
Figure 3.5	Unequal T-junction divider :(a) power split; (b) phase compensation; (c) impedance matching. [38]	28
Figure 3.6	Corporate power divider with unequal distribution [40]	28
Figure 3.7	Power tapering using number of power divider junction [43]	29
Figure 3.8	Rectangular microstrip antenna arrays. (a) Non-uniform spacing and amplitude. (b) Non-uniform spacing and uniform amplitude [44]	29
Figure 4.1	(**a**) Structure of the single patch with the parasitic element. (**b**) Gain of the patch with and without the parasitic patch in the x-z plane along theta (θ).	31
Figure 4.2	Linear patch array of an even number of elements with the excitation amplitude (a_n) of the nth antenna element and the distance (d_n) between n-1th and nth elements on the x–y plane. Excitation and spacing are set by symmetry ($a_{-n} = a_n$ and $d_{-n} = d_n$).	32
Figure 4.3	Normalized array factors of the 12-element array with (**a**) uniform amplitudes [1, 1, 1, 1, 1, 1] and uniform λ/2-spacing, (**b**) non-uniform amplitudes [1, 1, 0.707, 0.707, 0.707, 0.707] and uniform λ/2-spacing, and (**c**) non-uniform amplitudes [1, 1, 0.707, 0.707, 0.707, 0.707] and non-uniform spacing [0.459λ, 0.528λ, 0.454λ, 0.421λ, 0.548λ, 0.598λ].	33
Figure 4.4	(a) one-to-six way non-uniformly powered and uniformly spaced power divider. (b) Two one-to-six-way power dividers for 12 feeding ports to the antenna elements.	34
Figure 4.5	Phase delays from the input port to output ports 4, 6, 8, 10, 12 and 14 when (a) L1 = 16.37 mm and (b) L1 = 16.11 mm. (c) Normalized gain along theta (θ) of the 12 patch elements individually fed by the realized amplitudes and phases from the designed power divider and the ideal values.	35
Figure 4.6	(**a**) Top view of the non-uniformly powered and uniformly spaced 12-element patch array. (**b**) Simulated normalized gain of the non-uniformly powered and uniformly spaced 12-element patch array with co- and cross-polarization. (**c**) Simulated S_{11} of the same antenna array.	36
Figure 4.7	(**a**) Non-uniformly spaced 12-element patch array without a power divider. (**b**) Normalized gain of the non-uniformly powered and non-uniformly spaced patch array without a power divider in the simulation.	37
Figure 4.8	(a) One-to-six-way uniformly powered and spaced power divider. (b) 2-to-12 non-uniformly powered and spaced divider. (c) Normalized gain along theta (θ) of the 12 patch elements individually fed by the realized amplitudes and phases from the designed power divider and the ideal values.	38

Figure 4.9	**(a)** Top view of the non-uniformly powered and spaced 12-element patch array. (**b**) Simulated normalized gain of the non-uniformly powered and spaced 12-element patch array with co- and cross-polarization. **(c)** Simulated S_{11} of the same antenna array.	39
Figure 4.10	(**a**) Fabricated non-uniformly powered and uniformly spaced antenna array without parasitic patches. (**b**) Fabricated non-uniformly powered and spaced antenna array without parasitic patches.	40
Figure 4.11	(**a**) Fabricated non-uniformly powered and uniformly spaced antenna array with parasitic patches. (**b**) Fabricated non-uniformly powered and spaced antenna array with parasitic patches. **(c)** Wilkinson power divider for two output ports with 180° phase shift.	40
Figure 4.12	Simulation and measured S_{11} of (**a**) the non-uniformly powered and uniformly spaced antenna array, and (**b**) the non-uniformly powered and spaced antenna array.	41
Figure 4.13	Measurement Setup (**a**) Phase shifter with metallic box (**b**) Side view of antenna array and phase shifter	41
Figure 4.14	Normalized simulation and measurement gain of (**a**) the non-uniformly powered and uniformly spaced antenna array, and (**b**) the non-uniformly powered and spaced antenna array.	42
Figure 5.1	Uniform half-wavelength spaced array without power divider	45
Figure 5.2	Simulation of uniform spaced array without power divider (SLL= -16.77) (**a**) 10° (**b**) -10°	45
Figure 5.3	Simulation of uniform spaced array without power divider (SLL= -16.13) (**a**) 20° (**b**) -20°	46
Figure 5.4	Simulation of uniform spaced array without power divider (SLL= -15.27) (**a**) 30° (**b**) -30°	46
Figure 5.5	Simulation of uniform spaced array without power divider (SLL= -15.5) (**a**) 40° (**b**) -40°	46
Figure 5.6	imulation of uniform spaced array without power divider (SLL= -14.13) (**a**) 50° (**b**) -50°	47
Figure 5.7	Non-uniform spaced array without power divider	47
Figure 5.8	Simulation of non-uniform spaced array without divider (SLL= -18.93) (**a**) 10° (**b**) -10°	48
Figure 5.9	Simulation of non-uniform spaced array without divider (SLL= -18.60) (**a**) 20° (**b**) -20°	48
Figure 5.10	Simulation of non-uniform spaced array without divider (SLL= -18.15) (a) 30° (b) -30°	48
Figure 5.11	Simulation of non-uniform spaced array without divider (SLL= -16.62) (**a**) 40° (**b**) -40°	49
Figure 5.12	Simulation of non-uniform spaced array without divider (SLL= -11.42) (**a**) 50° (**b**) -50°	49
Figure 5.13	E Field at +50°for uniform array (circle represent low interception of E field)	50
Figure 5.14	E Field at +50°for non-uniform array (circle represent high interception of E field)	50

LIST OF TABLES

Table 3.1	Pascal's Triangle for Binomial Coefficient	23
Table 4.1	Required transmission coefficients, percentages of power, normalized power, and the excitation of the respective ports in the power divider for SLL reduction from Figure 4.4a.	34
Table 4.2	Simulated transmission coefficients, percentages of power, normalized power, and the excitation of the respective ports in the power divider for SLL reduction from Figure 4.4a.	34
Table 4.3	Phase delays from ports 4, 6, 8, 10, 12 and 14 after tuning L1 and L2, and adding the meander lines in the one-to-six power divider, as shown in Figure 7a.	38
Table 4.4	Performance comparison of the antenna arrays, fed by the microstrip-based power divider, operating near 28 GHz for 5G applications.	43

CHAPTER 1: INTRODUCTION

The goal of this chapter is to illustrate a framework and introduction of the research work. The whole chapter is divided into two sections motivation and goal, and the thesis organization.

1.1 Motivation and Goal

For a millimeter-Wave (mm-Wave) application side lobe level (SLL) reduction and high gain realization are the primary requisitions. Till date, numerous technique has been used for sidelobe level reduction. The non-uniform power distribution to the antenna elements is an effective way to lower the SLL. The Chebyshev, binomial, and Taylor distributions are adopted for a wide range of antenna applications over the last 50 years [1]. To adopt this distribution people usually taper the radiating elements or transmission line. However, tapering transmission lines or radiating elements leads to a high cross-polarization. In that case, numerous application needs a low cross-polarization for effective signal strength to the specified direction. In [2], a non-uniform amplitude tapering for low SLL was realized by using the level of the power divider of a corporate feed network. This technique does not need to taper the transmission line or radiating elements. Although this technique is adopted by simulation for 5.8 GHz, the practical implementation was not realized.

Our goal is to present a solution for low SLL in the mm-Wave application without tapering transmission lines or radiating elements. Due to the high path-loss in the mm-Wave regime, it’s not easy to minimize the SLL without tapering the transmission line or radiating element. It needs a very careful design approach and implementation. We propose an amplitude tapering technique for the mm-Wave regime by using the level of the power divider. In addition, we use a differential feeding technique to minimize mutual coupling between the adjacent antenna elements in the mm-Wave regime. We expect a considerable side lobe level reduction which can be used for mm-wave application as well as 5G application at 28 GHz.

1.2 Thesis Organization

Chapter 2 illustrates the fundamental theory of microstrip antenna and design formula in detail. Also, parasitic patch integration for high bandwidth and gain has been introduced in this chapter. The array integration needs a corporate or parallel feeding arrangement, this feeding technique with literature review has included in the later part. Finally, basic parameters for an antenna like radiation pattern, beamwidth, gain and efficiency, S-parameters, impedance matching, antenna array, and array factor description have been added to the final part of this chapter.

In Chapter 3, the background of this study for sidelobe reduction is discussed elaborately.

In chapter 4, the design of a non-uniformly excited and non-uniformly spaced power divider has been discussed. First, a single parasitic patch antenna was analyzed for high gain implementation. Second, the radiation pattern and side lobe level were discussed from the array factor calculation. Third, a non-uniformly excited and spaced power divider was designed and optimized for phase correction and implemented with a patch to form a linear array. As a counterpart, the uniformly powered and spaced array was designed to realize and compare the SLL with a non-uniformly spaced antenna array. The result from fabrication and measurement was discussed in the final part of this chapter.

Finally, in the 5th chapter, the overall outcome of the study are summarized as well as few suggestion and future works are also provided of this research.

CHAPTER 2: ANTENNA AND ANTENNA PARAMETERS

An antenna is a conducting structure which is used to transmit or receive electromagnetic power for the wireless communication purpose. Due to reciprocity, a specific antenna structure can be used for both transmitter and receiver. There are various shapes and sizes of antenna available as the dipole, loop, helix, the log-periodic, parabolic dish reflector, horn, microstrip antenna, and so on. This chapter illustrates the principle and design equation of the microstrip antenna with inset fed technique as well as parasitic patch implementation with corporate fed technique. This chapter also introduces some basic antenna parameters and the array factor of an antenna array. The whole chapter is divided into some sections which include the research background, the design equation, and a discussion about the figure of merit of the antenna.

2.1 The Microstrip patch Antenna

Microstrip antennas consist of a very thin metal patch with a ground plane separated by a narrow dielectric substrate. These antennas are widely used for low power applications, a low profile, low cost, and easy integration with microwave circuits. The microstrip antenna was first introduced by Deschamps [3] in 1953 and the patent was issued in 1955 [4]. However, it took 20 years to realize the considerable development in 1970 due to the availability of low loss substrate and ease of fabrication [5]. As shown in **Figure 2.1a**, the inset feeding configuration of the microstrip patch antenna has a radiating patch on one side of the substrate and the other side consisting of a ground plane [1]. The electric field distribution is shown in **Figure 2.1b** by the arrow line. The radiation is considered as the broadside of the radiation element (normal to the patch) as shown in **Figure 2.1c.** The electric field is zero at the center of the radiating element, maximum at one side where minimum on the opposite side. And the maximum and the minimum electric field continuously alternate their position according to the phase of the applied signal. The electric field does not stop suddenly at the periphery of the patch, instead, fields extend the outer periphery to some degree which is widely known as the fringing field. This fringing field is responsible for the patch to radiate. Generally, the radiating element can be arbitrarily any shape but the square, rectangular, and circular shape are widely used due to the ease of analysis, fabrication, and comparatively better radiation characteristics. The dielectric constant 'ε_r' of the substrate plays an important role to enhance the fringing field. There are numerous dielectric substrates available to design the microstrip antenna and the range of the dielectric constant is $2.2 \leq \varepsilon r \leq 12$, and substrates are chosen depending on the radiation, efficiency, and loss consideration [1].

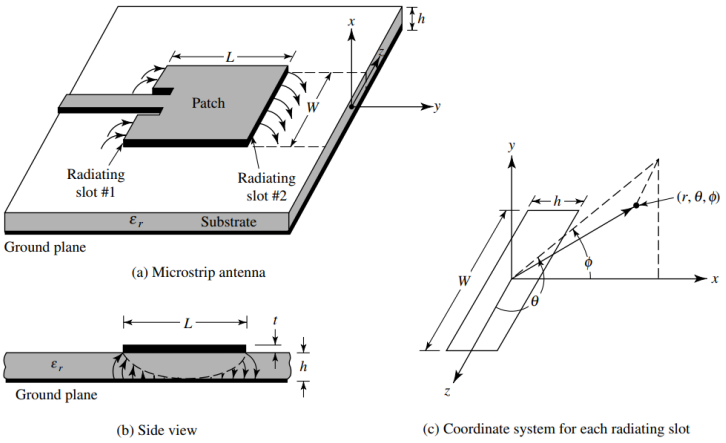

Figure 2.1 Microstrip antenna and corresponding coordinate system [4]

The height of the substrate is very narrow compared to the wavelength (h < < λo). The length 'L' of the patch has an impact on the resonance frequency and can be determined numerically. The length and width (L and W) of the patch antenna can be calculated by using the following **Equation 2.1**.

$$W = \frac{C}{2f_o\sqrt{\frac{\varepsilon_r+1}{2}}} \tag{2.1}$$

$$L = \frac{C}{2f_o\sqrt{\varepsilon_{eff}}} - 0.824h\left(\frac{(\varepsilon_{eff}+0.3)(\frac{W}{h}+0.264)}{(\varepsilon_{eff}-0.258)(\frac{W}{h}+0.8)}\right) \tag{2.2}$$

$$\text{where } \varepsilon_{eff} = \frac{\varepsilon_r+1}{2} + \frac{\varepsilon_r-1}{2}\left(\frac{1}{\sqrt{1+12(\frac{h}{w})}}\right) \tag{2.3}$$

Here, c is the speed of the light in free space

f_o = resonant frequency

ε_r =dielectric constant

ε_{eff} = effective dielectric constant

h = the height of the dielectric

W= width of the patch antenna

L = Length of the patch antenna

Once the dielectric constant, the height of the dielectric and resonant frequency specified we can easily determine the length and width of the patch by using **Equations 2.1, 2.2, and 2.3**. Besides, the length

and width can be optimized by using full-wave simulation software for different purposes. There are several feeding procedures available for microstrip patch antennas like coaxial probe feeding, aperture coupled feeding, proximity feeding, edge feeding, or inset feeding by microstrip line [6]. All of the feeding technique utilizes the input impedance matching with 50 ohms to minimize the reflected power from the radiating element. In this thesis, our interest is to work with inset feeding microstrip antenna as this feeding gives great flexibility to make an antenna array by parallel feeding technique.

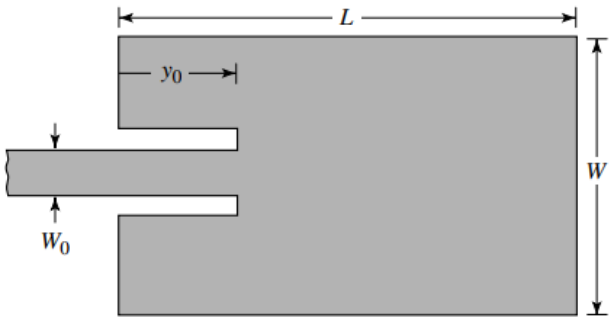

Figure 2.2 Inset feed micro-strip antenna

In an inset feeding antenna, a slot needs to cut along the longitudinal direction of the patch to connect with the 50-ohm feed line. The resonant impedance can be optimized by varying the length of yo as shown in **Figure 2.2**. The width of the 50-ohm feed line is W0 and the characteristic impedance of the feed line can be found by using **Equation 2.4.**

$$Z = \frac{60}{\sqrt{\varepsilon_{eff}}} ln\left(\frac{8h}{W_0} + \frac{W_0}{4h}\right) \qquad \text{if } \frac{W_0}{h} \leq 1 \tag{2.4}$$

The inset feeding length for 50 ohm can be approximated from **Equation 2.5** [4].

$$Z_{in}(y = y_0) = Z_{in}(y = 0)cos^2(\frac{\pi}{L}y_0) \tag{2.5}$$

From **Equation 2.5**, it is evident that the input impedance can be varied by changing the length of y_0. At the edge $y_0 = 0$, input impedance is maximum (Z_{in}). When we approach from the edge towards the center, the input impedance decreases and it becomes zero at the center of the patch $(\frac{L}{2})$. So from this discussion, we can approximate the 50-ohm feeding point in between the edge to the center of the patch. Another way to find the inset feeding length for 50 ohms can be approximated by using **Equations 2.6 and 2.7** shown in reference [7].

$$y_0 = \frac{L}{2\sqrt{\varepsilon_{eff}(L)}} \tag{2.6}$$

$$\varepsilon_{eff}(L) = \frac{\varepsilon_r+1}{2} + \frac{\varepsilon_r-1}{2}\left(\frac{1}{\sqrt{1+12(\frac{h}{L})}}\right) \tag{2.7}$$

Here L is the length of the patch antenna and $\varepsilon_{eff}(L)$ is the effective dielectric constant along length, ε_r is the dielectric constant of the substrate.

The microstrip antenna has been a popular choice due to low profile, low cost, less weight, low power, and easy integration with microwave circuits. In contrast, it possesses spurious radiation from the feed and has bandwidth limitations. However, during the last 50 years, the microstrip antenna has matured tremendously and many of their limitations have been overcome. The efficiency and bandwidth of the antenna can be increased by increasing the height of the substrate. But increasing the height of the substrate introduces the surface wave, which receives power from the system and causes degradation of the antenna radiation pattern, and polarization [8]. Such Surface wave propagation can be eliminated by using a photonic bandgap structure [9]. The gain and low power limitations can be eliminated by using an antenna array. The spurious radiation from feed can be minimized by using aperture coupling which has two physically separated functions. Now a day's bandwidth of the microstrip antenna can be enhanced by using various aperture shape feeding, stacking of the substrate, and by using the parasitic patches. The parasitic patch also increases the gain of the patch antenna which can be used for antenna array configuration.

2.2 The Parasitic Patch Antenna

The parasitic patch is known as a dummy element that is not connected to the source rather it is electromagnetically coupled with radiating elements. The parasitic patch is a popular choice for bandwidth and gain enhancement of the antenna. To date, numerous effort has been done to integrate different parasitic patches from microwave to mm-wave frequencies. The parasitic patch increases the bandwidth and gain due to the resonance coupling between the feeding patch and the parasitic patch. The parasitic antenna can be co-planar or stacked. In co-planar structure, parasitic elements are placed on the horizontal plane with the driven patch, and overall bandwidth can be increased when the resonant frequency of parasitic elements is slightly different than of the driven patch. Because overall frequency response can be the superposition of the frequency responses of the individual patch. The parasitic patch can be coupled via radiating or non-radiating edges as well as via both radiating and non-radiating edges

of the driven patch. In **Figure 2.3,** the example of the co-planar parasitic patch and VSWR plot was presented. Four parasitic patches are coupled via radiating and non-radiating edges and feeding were provided on the driven patch.

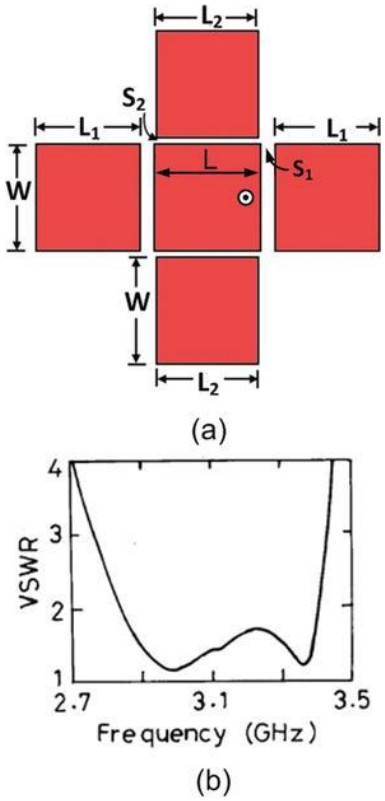

Figure 2.3 Co-planar four microstrip parasitic elements coupled via radiating and non-radiating edges a) antenna configuration b) VSWR plot presented in reference [10]

In 1980, a co-planar parasitic patch has introduced with λ/4 short circuit parasitic elements on both sides of the radiating sources which effectively doubled the bandwidth [11]. Another effective way to introduce parasitic patch is stacking, where the driven patch is placed vertically with another patch. The characteristic of this configuration mostly depends on the gap between the driven patch and the parasitic patch. When the gap is small enough the resonant frequency of the parasitic patch is slightly different than the parasitic patch and bandwidth becomes higher due to the superposition of two frequency functions. In **Figure 2.4**, the microstrip patches shown as the fed patch and the parasitic patch are separated by the gap 'hp' and are electromagnetically coupled with each other [12].

In 1981, Oltman and Huebner first introduced the electromagnetically coupled microstrip radiators by stacking dipole closely to the microstrip feed line [13]. They achieved bandwidth 2.5 to 5.5

percent with VSWR 1.92. Two years later in 1983, Sabban introduced high bandwidth (9 to 15 %), a double layer stack antenna with circular, square, and rectangular configuration [14].

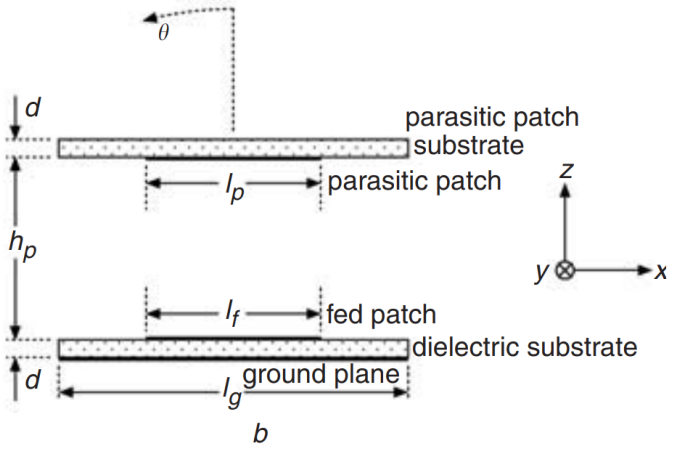

Figure 2.4 Stack microstrip Patch [12]

A broadband two-layer microstrip antenna was introduced with higher bandwidth and 1.2 VSWR for circular polarization in [15]. In [16], the three-layer triangular structure was employed to increase the bandwidth of up to 17.5%. In 1988, two overlying parasitic directors are stacked to enhance the gain from 4.7 dB to 10.6 dB and half-power beamwidth also decreased significantly from 103° to 30° [17]. In [18], the gain was found the maximum when the gap between the driven patch and parasitic patch is approximately 0.31λ0. However, another experiment shows that the sizes of the parasitic patch have a great impact on the resonant frequency, input impedance, and bandwidth. For broadband antennas, the maximum gain was realized when the parasitic and the fed patch are equal in size [19]. In contrast, it's possible to achieve high gain and high bandwidth simultaneously by two parasitic elements. A stacked three-element antenna was designed and investigated experimentally using two parasitic patches, one which increases bandwidth (up to 10 %) and another patch increases gain 8 -11.7 dB [20]. Apart from the high gain and bandwidth, a multi-frequency (5 bands) microstrip patch antenna was introduced where four parasitic patches with the single driven patch were integrated [21]. This antenna provided great flexibility for pentaband operation with stable gain characteristics. In [22], a stacked microstrip antenna with thick parasitic patch substrate was investigated experimentally and the maximum gain was realized when the gap between the driven patch and parasitic patches was found 0.5 λg (guided half wavelength). Till 2004, there was no systematic approach to synthesis the dual behavior of a parasitic patch for being broadband and high gain. Finally, it was summarized that the characteristic of the

stacked patch antenna depends on the gap between the driven patch and parasitic patch [12]. When fed patch and parasitic patches are close enough they form two near-resonant frequencies because the resonant mode of the parasitic patch is close to the primary mode of the fed patch. When the distance between these patches increases to 0.5 λg then two resonant frequencies dis-appears and the antenna acts as a leaky resonator. Hence, the gain of the antenna increases. There exist two types of resonator depending on the distance between the patches. However, literature provides adequate knowledge for gain and bandwidth enhancement, but a single antenna configuration cannot meet the demand for high gain. The high gain can be realized by the antenna array configuration. The parallel feeding arrangement is one of the effective ways of arranging the antenna array.

2.3 The corporate (parallel) feeding

The microstrip fed network (corporate or parallel) consists of two-way power splits of input power, and the equal length of the transmission line provides an equal phase to all output ports. Generally, the corporate feed network realizes an equal power split where the number of the output port is 2n, where n is the number of levels of power split. According to this number of output port can be 2, 4, 8, 16, and 32, and so on. In contrast, unequal power split can be realized by using a parallel feeding technique where the number of output feeds can be 6, 12, and so on. The initial development of the microstrip array was conducted by Munson in 1973 [23-24]. Munson excited a metal strip (wrap-around) for an omnidirectional radiation pattern by using a corporate feed network at several points of the metal strip. The spacing was chosen as less than a guided wavelength (λg). There are two ways to construct corporate feed, generally a tapered feed transfer 50 Ω impedance to 100 Ω which can be combined with another 100 Ω line for the impedance matching purpose shown in **Figure 2.5 (a).** Another way is to use the quarter-wave impedance transformer to transfer the impedance to 50 Ω to match with the input feed line as shown in **Figure 2.5 (b).** There has several quarter-wave transforms on the figure for impedance matching. The quarter-wave impedance transformation can be done by calculating the impedance using **Equation 2.8**.

$$Z_{\frac{\lambda}{4}Transformer} = \sqrt{Z_{in}Z_{out}} \tag{2.8}$$

Once input and output impedance is known then the impedance of the quarter-wave transformer can be determined and the width of the transmission line can be adjusted for the required characteristic impedance.

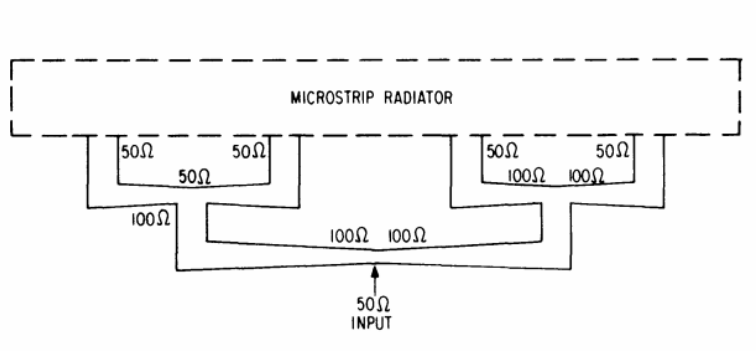

(a)

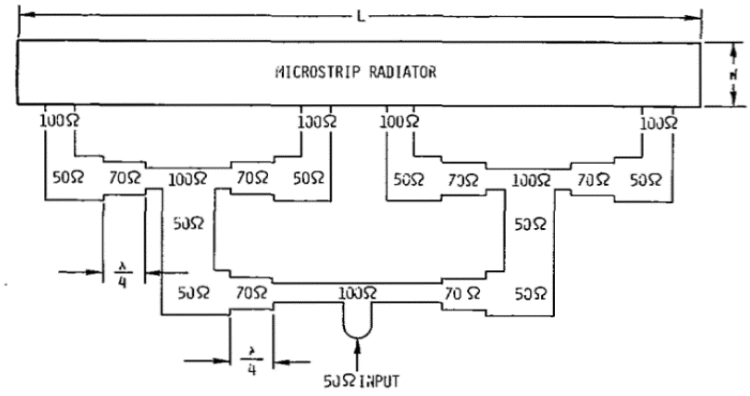

(b)

Figure 2.5 Corporate feed a) Realization by tapered line b) using the quarter wave transformer [23]

Several corporate feeding arrays were demonstrated for different phased array applications. To minimize the mutual coupling between any two junctions the separation from one junction to another needs to be at least half of the guided wavelength [25]. The mutual coupling of radiating elements affects the radiation pattern of the antenna array. To compensate for the mutual coupling of radiating elements, the distance d9 shown in **Figure 2.6** need to adjust.

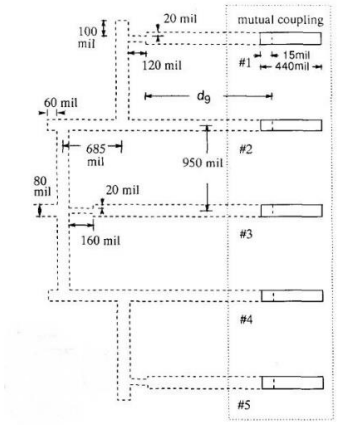

Figure 2.6 Corporate feed five element dipole array (mutual coupling considered inside the dotted box) [25]

2.4 Antenna Parameters

The parameter which associated with electrical and magnetic properties of an antenna include radiation pattern, gain, bandwidth, antenna efficiency, s-parameters, input impedance, and voltage standing wave ratio (VSWR). All of these parameters are described in the following section.

2.4.1 Radiation Pattern

An antenna radiation pattern is a graphical representation of radiated power measured at a certain distance from the radiating elements [1]. The graphical representation is a three-dimensional plot which represents the power density as a function of direction (zenith angle Θ and azimuth angle Φ). The radiation pattern can be realized as decibel (dB) by normalizing the power density in a specific direction. The 3-D pattern of the radiation field of an antenna is shown in Figure 2.7. The radiated lobes are divided into two groups. The first one is the main lobe or major beam is directed to the direction of the antenna radiation. The 2nd lobe is called the minor lobes where power density is very low compared to the major lobe. Besides, minor lobes are further divided into two groups, the first one is the side lobes and another one in the back lobe. Side lobes are situated near the main lobe. The back lobe is situated exactly to the opposite of the major lobe. For many applications, the ultimate design goal of an antenna is to reduce the side lobes as much as possible so that the major lobe possesses maximum power for better radiation.

2.4.2 Beamwidth

The angle between two similar points on the opposite side of the radiation maxima is called the beamwidth as shown in **Figure 2.7** [1]. There are two types of beam width, one is half-power beamwidth (HPBW), and another is the first null beamwidth (FNBW). The half-power beamwidth is defined as the beamwidth of half power point of radiation maxima or widely known as 3dB beamwidth. The angular separation between the first null of the radiation pattern is defined as the first null beamwidth (FNBW).

2.4.3 Directivity

Directivity of an antenna is defined as the ratio of maximum radiation intensity to the average radiation intensity or the total radiated power over 4π space. In simple form, directivity can be represented in a mathematical term as **Equation 2.9**.

$$D = \frac{U_{max}}{U_{ave}} = \frac{4\pi\, U_{max}}{P_{rad}} \tag{2.9}$$

Here,

D= Directvity

*U*max = maximum radiation intensity (W/unit solid angle)

Uave = average radiation intensity (W/unit solid angle)

*P*rad = total radiated power (W)

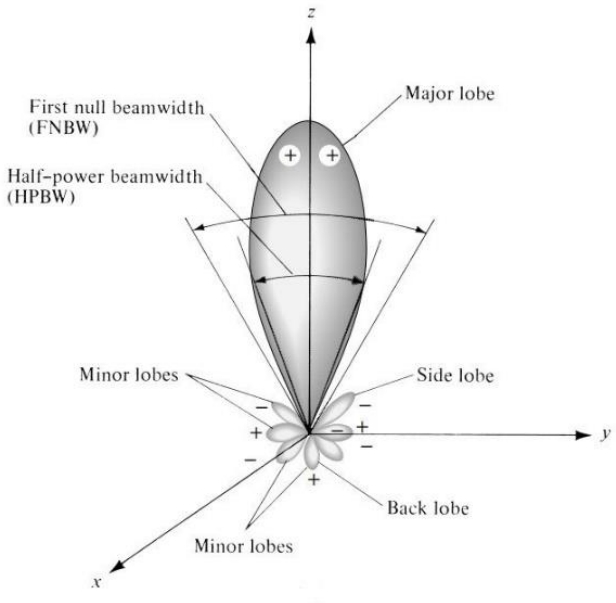

Figure 2.7 Radiation pattern and Beamwidth of antenna [25]

2.4.4 Antenna Gain

The antenna gain is defined as the power concentration to the direction of antenna radiation which is the ratio of radiation intensity to the total input power over 4π space. In contrast with directivity, antenna gain consider the ohmic losses and impedance mismatch in the antenna. Because total input power is considered for gain realization, here total power is the summation of radiated power and losses of the antenna. But, directivity considers radiated power only. So directivity will be always higher than gain. The gain is calculated by **Equation 2.9**.

$$Gain = \frac{4\pi\ Radiation\ Intensity}{Total\ Input\ Power} = \frac{4\pi\ U(\Theta.\Phi)}{P_{in}} \quad (2.10)$$

2.4.5 Antenna Efficiency

Antenna efficiency is defined as the ratio of radiated power over input power.

$$Efficiency, \eta = \frac{P_{rad}}{P_{in}} \quad (2.11)$$

2.4.6 S-parameters (Reflection Coefficient) and Bandwidth

The important parameter of an antenna is the reflection coefficient or S11. The S11 is defined as the reflected power of the antenna due to the impedance mismatch between the radiating element and the waveguide or transmission line. Generally, S11 is measured as dB (decibel), where -10 dB means 10 % of input power is reflected in the source. The lower value of S11 defines the better impedance match of a device and indicate lower reflected power to the source. The bandwidth of an antenna defines the span of the frequency band where the reflection coefficient is lower than -10 dB. The high bandwidth is one of the requirements for broadband application.

2.4.7 VSWR (Voltage Standing Wave Ratio)

VSWR stands for voltage standing wave ratio which is defined by the ratio of voltage maxima to voltage minima of a standing wave formed in a close loop or a system if there exists a reflected wave. It also describes the measurement of the percentage (%) of power which is being reflected. It can be defined mathematically by S11 as $VSWR$ = (1 - | S11|)/(1 + | S11|). For the ideal antenna, VSWR is 1.0 that means that power is not reflected back from the antenna. Generally, the antenna with the VSWR range 1.0 to 2.0 is desired for practical application.

2.5 Antenna Array and Array Factor

The radiation pattern of the single antenna is very wide and directivity and gain are low for such an antenna. For long-distance communications sometimes it's necessary to build an antenna with high directivity (high gain). One way is to increase the directivity of the antenna is to enlarge the antenna size, but practically it's difficult to build a big antenna due to its high cost. One of the simple ways to enlarge the antenna by arranging a single antenna in an orderly fashion which will effectively increase the gain of the system. These orderly arranged antennas are referred to as antenna array as shown in **Figure 2.8**. The total radiated field of the array is the vector addition of the individual elements to the specific direction. For high directivity in a specific direction, the field from individual elements needs to make constructive interference wherein the field to the other direction needs to be destructive. The individual elements of the antenna array can be identical or non-identical, it depends on the application and requirement. In an identical element array, there have the following parameters that effectively determine the shape of the radiation pattern [1].

1. The physical shape of the array (linear, circular, rectangular, spherical, etc.)
2. The distance between the elements
3. The excitation amplitude of the individual elements

4. The excitation phase of the individual elements

5. The radiation pattern of the individual elements

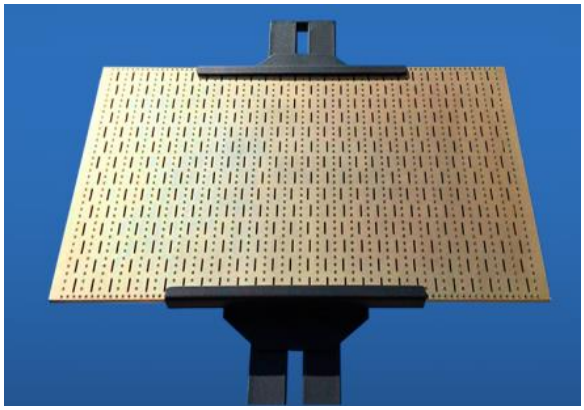

Figure 2.8 A Planar Antenna Array [26]

The total field of an antenna array is equivalent to the field of a single element multiplied by a factor known as array factor. The array factor of an antenna array determines the overall radiation pattern of the array and it is the function of the geometry of the array and the phase [1]. The total array pattern can be written as following.

Array Patter = Pattern of single element × Array factor.

The array factor (AF) of n element array as shown in **Figure 2.9** can be realized by the **Equation (2.12)**, for brevity we are not providing the derivation of the array factor.

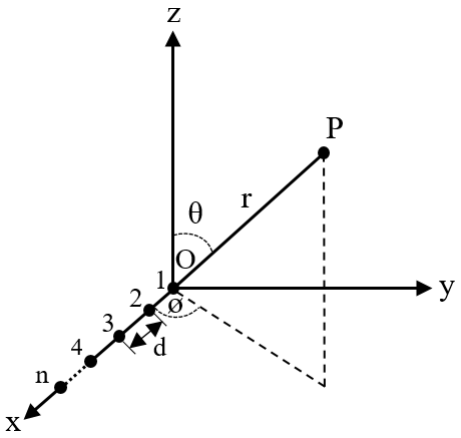

Figure 2.9 An N-element antenna array along x axis

$$AF(\theta) = \sum_{n=1}^{n} a_n e^{jnkd\sin(\theta)} \qquad (2.12)$$

Here, AF is the array factor

n, the index for the antenna element

a_n is the nth element's excitation amplitude,

d is the interelement spacing

k is the wavenumber = $2\pi/\lambda$,

θ is the elevation angle from the *z* axis.

The two most important parameters of the antenna array are interelement spacing (d) and the phase. Generally, the interelement spacing of the antenna array needs to be lower than one wavelength by avoiding the mutual coupling between the antenna elements. Because one wavelength spacing creates grating lobes to the unwanted direction due to the constructive interference of individual elements, rather than the direction of the main lobe [1]. The phase of the individual elements plays an important role in the beam steering application. A phased array can be constructed by providing the progressive phase shift to the individual elements in the array. In contrast, the amplitude of the individual element plays a vital role in the power distribution towards the main lobe and the minor lobe in the radiation pattern. The non-uniform amplitude provides a lower minor lobe for a specific arrangement of the antenna array. This non-uniform amplitude can be realized by a tapering technique developed within the last 50 years. We will discuss some tapering technique for lower side lobe level realization in the next chapter

CHAPTER 3: LITERATURE REVIEW FOR ARRAY WITH LOWER SIDE LOBE LEVEL

3.1 SLL Reduction Technique

Generally, there are three amplitude distribution named uniform, Binomial, and Chebyshev distribution. The Binomial and Chebyshev distributions are non-uniform amplitude distribution used for different applications with low SLL. The uniform amplitude distribution has the lowest half-power beamwidth compared to the Binomial and Cheybeshev distribution. On the other hand, Binomial distribution with element spacing equal to λ/2 or less than λ/2 has no sidelobe level. In this chapter, we aim to elaborate discussion to minimize the SLL by amplitude tapering. First, we will discuss Binomial and Chebyshev distribution. Then we will shortly discuss the millimeter-Wave application requirement with transmission line and radiating element tapering technique. Finally, the realization of non-uniform amplitude distribution will be discussed by using the number of the power level of a corporate feeding network.

3.1.1 Binomial Distribution

J. S. Stone [27], first suggested the procedure to determine the excitation coefficient. A binomial expansion can be written for a function $(1+x)^{m-1}$.

$$(1+x)^{m-1} = 1 + (m-1)x + \frac{(m-1)(m-2)}{2!}x^2 + \cdots \quad (3.1)$$

The coefficient for different value of m can be written as Pascal's triangle law shown in **Table 3.1**.

Table 3.1: Pascal's Triangle for Binomial Coefficient

m = 1					1					
m = 2				1		1				
m = 3			1		2		1			
m = 4		1		3		3		1		
m = 5	1		4		6		4		1	
m = 6		1		5		10		10		5		1
m = 7			1		6		15		20		15		6		1
m = 8		1		7		21		35		35		21		7		1
m = 9	1		8		28		56		70		56		28		8		1
m = 10	1		9		36		84		126		126		84		36		9		1

Here m represents the number of elements of the array and the coefficient represents the relative amplitude of the respective elements. This is called a binomial distribution. A binomial array of elements spacing λ/2 does not have a minor lobe but they have high beam width compared to uniform or Chebyshev array. So there is always a tradeoff between the beam width and minor lobe for the binomial array. Another disadvantage for a binomial array is wide variations between the amplitude of the different elements of the array. It can be understood from Pascal's triangle, the amplitude of the end elements of the 9-element array is 1, and the middle element is 70. That's why it's quite inefficient to design and maintain an array with this large variation of amplitude distribution. And this is practically difficult to implement and it leads to the low efficiency of the feed network.

3.1.2 Chebyshev Distribution

Chebyshev distribution or Dolphe-Tschebyshev array is one of the widely used array patterns for numerous practical applications. This was first introduced in 1946 by Dolph [28] which is the compromise of uniform and binomial distribution. Due to the practical difficulties of binomial distribution Chebyshev distribution is considered for wide application. The array factor for even and the odd number of elements can be written as following [29].

$$(AF)_{2N}(even) = \sum_{n=0}^{N-1} I_n \cos(2n+1)u \tag{3.2}$$

$$(AF)_{2N+1}(odd) = \sum_{n=0}^{N} I_n \cos(2nu) \tag{3.3}$$

These two equation can be reduced to the polynomials of variable, x= cos u. To obtain the polynomial

$$e^{jnu} = (\cos nu + \mathrm{j} \sin nu)$$

For which it can be written as

$$\cos nu = cos^n u - n_{c_2} cos^{n-2} u\, sin^2 u + n_{c_4} cos^{n-4} u\, sin^4 u + \ldots\ldots \tag{3.4}$$

If trigonometric identity, then is a polynomial of degree n in x= cos u. Here each cosine term can be written as a series of cosine function.

n= 0 $\cos nu = 1 = T_0(x)$

n= 1 $\cos nu = \cos u = x = T_1(x)$

n= 2 $\cos nu = \cos 2u = 2\,cos^2 u - 1 = 2x^2 - 1 = T_2(x)$

n= 3 $\cos nu = \cos 3u = 4\,cos^3 u - 3\cos u = 4x^2 - 3x = T_3(x)$

n= 4 $\cos nu = \cos 4u = 8\,cos^4 u - 8\,cos^2 u + 1 = 8x^4 - 8x^2 + 1 = T_4(x)$

n= 5 $\cos nu = \cos 5u = 16\,cos^5 u - 20\,cos^3 u + 5\cos u = 16x^5 - 20x^3 + 5x = T_5(x)$

Here array factor is the summation of each of the cosine term and the unknown variable (excitation) of the array factor can be determined by equating the original Tschebyshev polynomial. And each of the cosine forms is related to Chebyshev polynomial. These relation between Chebyshev polynomial and cosine function are valid only in -1 ≤ x ≤ +1. The recursion formula can be written as

$$T_n(x) = 2xT_{n-1}(x) - T_{m-2}(x). \tag{3.5}$$

This equation is effective for each polynomial when the previous two are known. A Chebyshev array can be formed when the distance between the elements and the side lobe level (dB) is specified, and the excitation coefficient and the corresponding array factor can be calculated. For a specific minor lobe, the maximum distance between the elements can be calculated by equation 17 for Θ = 0 ° and Θ= 180°.

$$d_{max} \leq \frac{\lambda}{\pi} cos^{-1}(-\frac{1}{x}). \tag{3.6}$$

And the most widely used procedure to calculate the excitation amplitude using the computer is introduced by Barbiere [30], which is obtained using the following equations.

$$a_n = \sum_{r=n}^{N} (-1)^{N-r} x^{2r-1} \frac{(r+N-2)!\,(2N-1)}{(r-n)!\,(r+n-1)!\,(M-r)!} \tag{3.7}$$

For even 2N elements n=1, 2, 3…..N

$$a_n = \sum_{r=n}^{N+1} (-1)^{N-r+1} x^{2(r-1)} \frac{(r+N-2)!\,2N!}{\varepsilon_n\,(r-n)!\,(r+n-2)!\,(M-r+1)!} \tag{3.8}$$

For odd 2N+1 elements n=1, 2, 3…..N+1

And $\varepsilon_n = 2\ for\ n = 1$

$\varepsilon_n = 1\ for\ n \neq 1$

3.2 Radiating Elements Tapering

The binomial or Chebyshev technique can be applied by tapering the radiating elements. In [31], a series-fed binomial distribution was realized by tapering the radiating elements of 5 elements array, and SLL was reduced to -28 dB. As a counterpart, a uniform amplitude array was analyzed and SLL was found as -14.5 dB, both configurations are shown in **Figure 3.1**.

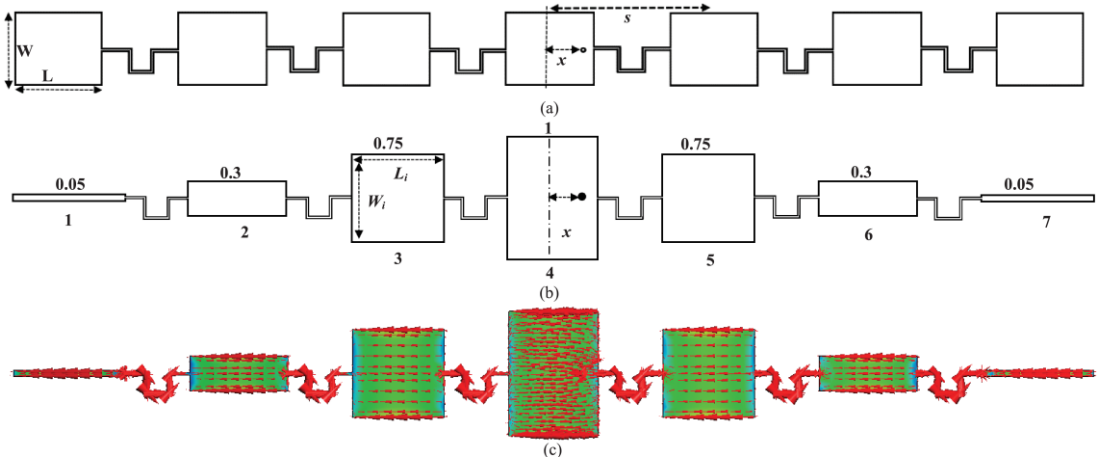

Figure 3.1 Array (a) identical elements (b) tapered patch width and (c) tapered patch current distribution [31]

A slotted SIW leaky-wave antenna was formed by tapering the slotted antenna for SLL reduction to -20 dB at the end-fire direction with maximum gain [32]. In [33], a cosine square distribution was realized by tapering the 8-element rectangular patch corporate-fed array where SLL was achieved -18.6 dB as shown in **Figure 3.2.** Similarly, a non-identical rectangular microstrip array was introduced by the series-fed method to achieve SLL -16.25 dB [34]. In contrast, to achieve Chebyshev distribution for -20 dB SLL both feed line and patch width tapering were used in [35] as shown in **Figure 3.3.** Besides, only transmission line tapering can achieve substantial SLL reduction which are discussed in the following.

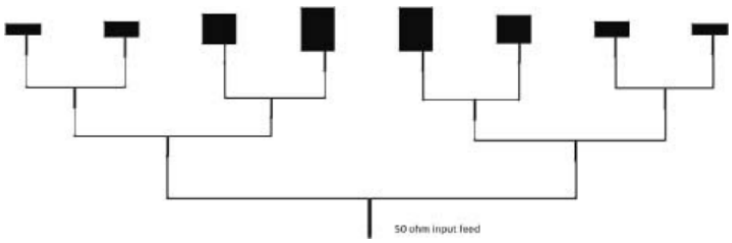

Figure 3.2 Different width Rectangular array with parallel feeding [33]

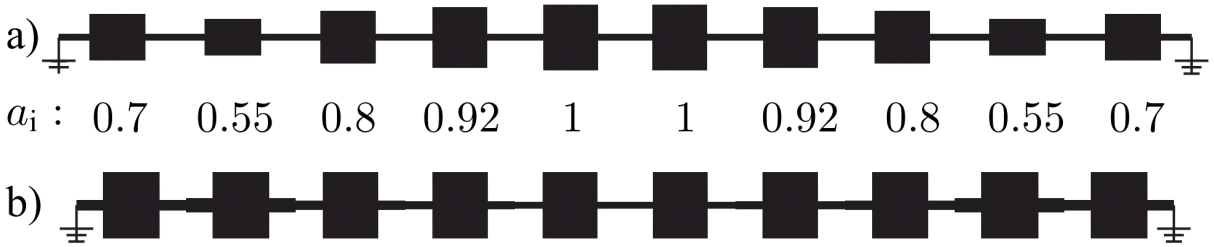

Figure 3.3 Configurations of array. a) Patch width-tapering; b) line-width tapering [35]

3.3 Transmission Line Tapering

Corporate feed power dividers with an unequal power division ratio can effectively reduce the SLL. The key is to provide the non-uniform amplitude to the individual antenna elements. This can be done by tapering transmission line. In a series-fed patch array, the characteristic impedance of the feeding microstrip line was tuned [36]. The power dividers with an unequal power division ratio in the T-junctions of the substrate integrated waveguide (SIW) are commonly used in the millimeter-wave band for amplitude tapering [37–42]. To achieve the non-uniform power distribution metallic post inserted on the junction of the divider and the shifting of these post changes the power dividing the ratio between two output ports as well as the phase and impedance matching can be obtained [37-39]. **Figures 3.4 and 3.5** illustrate the configuration and power diving principle of such an array. On the other hand, an SIW based un-equal power dividing ratio can be obtained by tapering the feed line [40-42]. The example of this arrangement is shown in **Figure 3.6** [40].

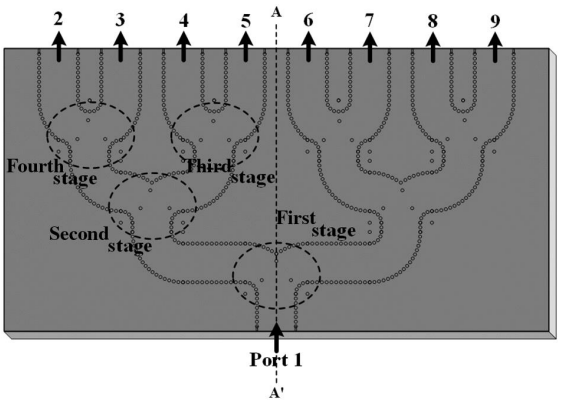

Figure 3.4 Configuration of SIW unequal 8-way power divider [38]

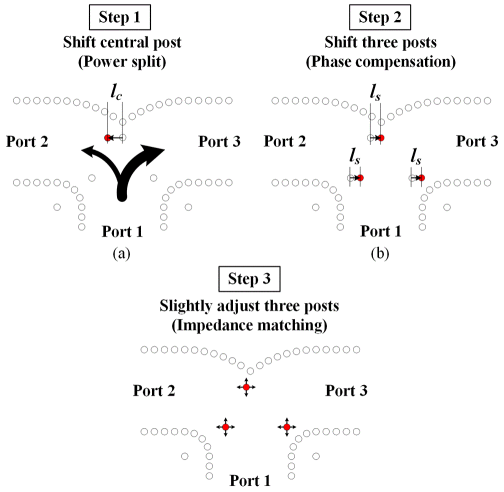

Figure 3.5 Unequal T-junction divider :(a) power split; (b) phase compensation; (c) impedance matching. [38]

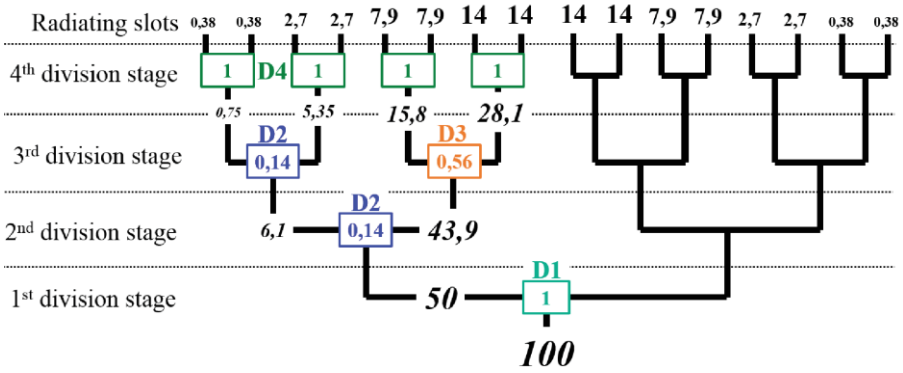

Figure 3.6 Corporate power divider with unequal distribution [40]

3.4 Tapering by Number of Power Level

The number of power dividing junctions from the input to each output (the level of the power split) in the microstrip line and SIW was controlled for tapering amplitude [39,43]. The performance of this power divider type mainly depends on the power split level for each output; therefore, the power divider's design process can be simple, and its sensitivity to fabrication uncertainty can be low. This arrangement does not necessarily taper the transmission line, only the number of power splitting junction determines the unequal power dividing ratio. A power divider for 12 elements of the array is shown in **Figure 3.7**, in which the middle 4-elements of the array will receive twice power compared to the power received by the rest 8 elements on the edge of the array.

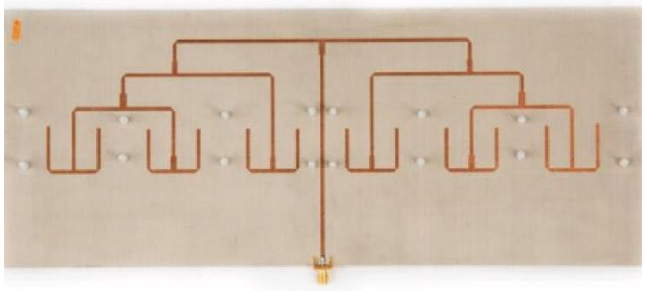

Figure 3.7 Power tapering using number of power divider junction [43]

3.5 Non-Uniform Spacing for SLL Reduction

The array factor is the function of spacing and excitation. The spacing variation can also realize the SLL reduction for an array. In [44,45], non-uniformly spaced series-fed arrays were introduced to reduce SLL at 9 GHz and 24 GHz, respectively, but these arrays also need to taper the radiating elements. A non-uniformly spaced elliptical array of 8, 12, and 20 elements with uniform excitation was designed, and nearly -20 dB SLL was verified in the numerical simulations [46]. The SLL reduction was realized by uniform and non-uniform spacing of the array as shown in Figure 3.8.

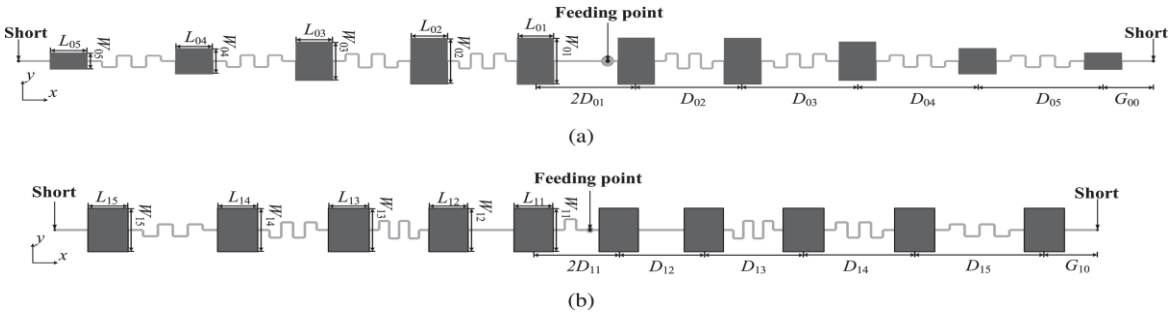

Figure 3.8 Rectangular microstrip antenna arrays. (a) Non-uniform spacing and amplitude. (b) Non-uniform spacing and uniform amplitude [44]

3.6 Requirement of Millimeter-Wave Antenna

In the mm-wave regime, the path loss is the widely pronounced matter, high gain and low SLL is the requirement for this frequency band. In the previous section, several approaches were discussed to reduce the SLL. Here, our goal is to design a power divider which can be effectively used for 5G application as well as mm-Wave application at 28 GHz. Our approach will be discussed which will cover the design procedure without tapering the transmission line, and for high gain and bandwidth requirement, the parasitic patch was also introduced. The design procedure and analysis are presented in the next chapter elaborately.

CHAPTER 4: NON-UNIFORMLY POWERED AND SPACED CORPORATE FEEDING ANTENNA ARRAY

4.1 Introduction

Millimeter-wave band systems have been actively studied for fifth-generation (5G) smartphones, which will provide higher data rates and capacity [47–49]. However, the millimeter-wave experiences high path loss; therefore, 5G-related hardware needs to increase the gain of the transmitter and receiver systems [50–52]. With a limited power resource, a directive antenna system that focuses energy in a specific direction with a sharp pencil beam is considered key hardware in millimeter-wave applications. The sharp beam can be realized by a high-gain antenna with a low sidelobe level (SLL) that requires an array of antenna elements.

In a patch antenna array, a popular antenna topology for millimeter-wave systems, parasitic patches have been implemented on a feeding patch array with a spacer to further increase the antenna gain [53–55]. Despite the increased gain from the parasitic patches, a main-beam offset in the E plane due to the near-field coupling between the parasitic and feeding patches was identified, and out-of-phase feeding to adjacent patches in the opposite feeding position was used as a solution [56]. In [56], an antenna array with 16 patches achieved 19.88 dBi gain, with the maximum beam at the boresight near 28 GHz; however, the array did not utilize methods to reduce SLL, and the value was limited to −13.4 dB. The other dipole, patch and aperture antenna arrays for 5G millimeter-wave applications also showed limited SLL values near −10 dB to −15 dB [57–61].

In [62], 12 patch elements, fed by a non-uniformly spaced power divider with amplitude tapering using different levels of power split in each output, achieved nearly −20 dB SLL at 5.8 GHz. However, the result was only verified in the numerical simulation, and a microstrip line-based power divider with non-uniform spacing is yet to be designed in the millimeter-wave band, and its SLL reduction has not been verified experimentally.

In this paper, we present a non-uniformly spaced microstrip line-based power divider to feed 12 patch antennas with amplitude tapering using different levels of T-junctions, and demonstrate the SLL reduction at 28 GHz experimentally. Differently from [62], the feeding network utilized two one-to-six unequally split power dividers, fed from the opposite side with out-of-phase, to maintain the maximum beam at the boresight by reducing mutual coupling among adjacent antenna elements. In addition, the patch antenna implemented the parasitic patch to increase gain for practical applications; therefore, non-uniform spacing for the lowest SLL was determined using full-wave simulations instead of the analytical array factor. Despite the non-uniform spacing between the antenna elements, the power

divider should maintain in-phase excitation for all the antenna elements. This design challenge was tackled by the T-junction position and the delay line optimization. As a counterpart to the non-uniformly powered and spaced power divider, we also designed a non-uniformly excited but uniformly spaced power divider for the same number of patches in order to prove SLL reduction from a non-uniformly spaced array effectively. In this paper, we first introduce a single patch antenna with parasitic elements for maximum gain. Then, the design procedure for both non-uniformly powered dividers with uniform and non-uniform spacing will be followed. Finally, we demonstrate the performance of the power dividers by analyzing the gain and SLL values of both antenna arrays in the simulation and measurement.

4.2 Design and Optimization of Antenna Array

4.2.1 Design of Single Patch with Parasitic

We designed a single patch antenna with a parasitic patch, as shown in **Figure 4.1a**. The parasitic patch mounted on the driven patch realizes resonance coupling, and hence the bandwidth and gain of the design can be improved [63]. In the design, two equally sized 7 × 7 mm^2 substrates, S_1 and S_2, were placed with an air gap of 1 mm to separate the driven and parasitic patch. A thin Rogers 5880 substrate with a thickness of 0.127 mm, dielectric constant of 2.2, and loss tangent of 0.0009 was used for both patches. The driven patch and parasitic patch were each 3.6 × 2.9 mm^2 in size. On the driven patch, the inset feed length and width were 0.45 mm and 1.1 mm, respectively, for 50 Ω matching. The simulated gain values of the patch antenna on the x-z plane with and without the parasitic patch are presented in Figure **4.1b,** illustrating the 1.63 dB increased gain of the patch antenna at 28 GHz due to the parasitic element. A commercial full-wave simulation tool, the high-frequency structure simulator (HFSS), was used to model the patch antenna and the following power dividers [64].

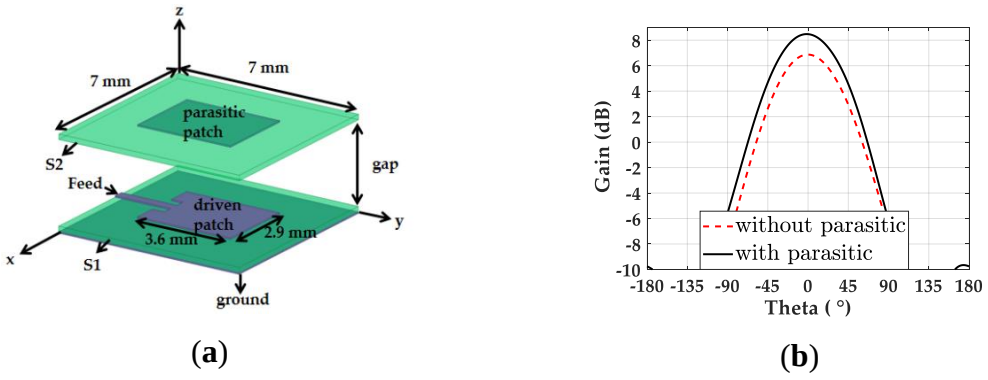

Figure 4.1. (**a**) Structure of the single patch with the parasitic element. (**b**) Gain of the patch with and without the parasitic patch in the x-z plane along theta (θ).

4.2.2 Effect of Non-Uniform Excitation and Spacing on SLL

We calculated the array factor using the excitation amplitudes and inter-element distances of 12 antenna elements, and found the optimum distances with a given tapered amplitude condition for the lowest SLL. Instead of 8 or 16 elements that opt to be equally powered, the 12-element array was chosen because a corresponding feed network can realize a non-equal output power with different power split levels. The array factor formula for the 12-element linear array is shown in **Equation (11).**

$$AF(\theta) = \sum_{n=-6}^{6} a_n e^{jkx_n \sin(\theta)} \quad (20)$$

Here, n, the index for the antenna element, has a range between −6 and 6, with an increment of 1, and n = 0 is excluded. a_n is the nth element's excitation amplitude, x_n is the location of the nth element along the *x* axis, k is the wavenumber, and θ is the elevation angle from the *z* axis. x_n was determined by d_n, the distance between n-1th and nth elements, and d_1 means the distance between two central patches in the array, as shown in **Figure 4.2.** For simplicity, we only defined a_n and d_n for positive n, and negative n cases were set by symmetry using $a_{-n} = a_n$ and $d_{-n} = d_n$.

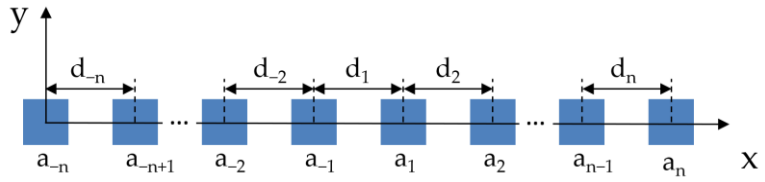

Figure 4. 2. Linear patch array of an even number of elements with the excitation amplitude (a_n) of the nth antenna element and the distance (d_n) between n-1th and nth elements on the x–y plane. Excitation and spacing are set by symmetry ($a_{-n} = a_n$ and $d_{-n} = d_n$).

The normalized amplitudes of the six elements for a uniform amplitude array (ULA) were set to be [a_1, a_2, …, a_6] = [1, 1, 1, 1, 1, 1]. For a non-uniformly excited array with a lower SLL, the normalized power levels of two-thirds of the elements were tapered, with [1, 1, 0.5, 0.5, 0.5, 0.5] using one more half-power division for n = 3, 4, 5 and 6. Therefore, the corresponding non-uniform amplitudes were set to be [a_1, a_2, …, a_6] = [1, 1, 0.707, 0.707, 0.707, 0.707]. With this amplitude condition, we searched the distances (d_n) between the patch elements, which provide the lowest SLL near the half-lambda distance with a +/− 0.1 lambda gap. Finally, non-uniform distances [d_1, d_2, …, d_6] = [0.459λ, 0.528λ, 0.454λ, 0.421λ, 0.548λ, 0.598λ] provided the lowest SLL of –20.90 dB, and the optimum distances show similar values to those previously reported for the 12-element array structure [30]. **Figure 4.3a** shows the normalized array factor of the uniformly (0.5λ) spaced ULA of 12 antenna elements along theta (θ), indicating an SLL of −13.07 dB. In **Figure 4.3b**, the non-uniform amplitude excitation of [1, 1, 0.707,

0.707, 0.707, 0.707] with uniform spacing (0.5λ) provides a ~3.5 dB lower SLL of −16.55 dB, compared to the ULA case. Finally, **Figure 4.3c** demonstrates that a minimum SLL value of −20.90 dB is possible with the non-uniformly powered and spaced antenna array. The array factor calculations verify that the optimum non-uniform distances between the antenna elements further reduce the SLL. In the next sections, the physical realization of power dividers for the 12-element patch array operating at 28 GHz will be presented.

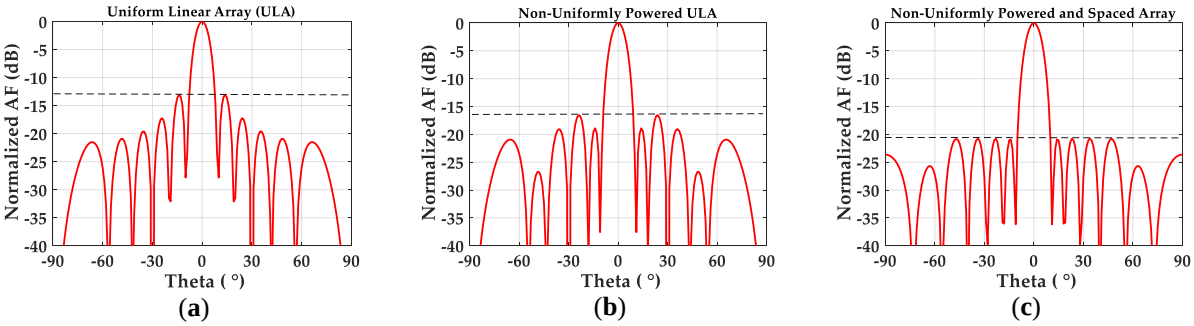

Figure 4.3. Normalized array factors of the 12-element array with (**a**) uniform amplitudes [1, 1, 1, 1, 1, 1] and uniform λ/2-spacing, (**b**) non-uniform amplitudes [1, 1, 0.707, 0.707, 0.707, 0.707] and uniform λ/2-spacing, and (**c**) non-uniform amplitudes [1, 1, 0.707, 0.707, 0.707, 0.707] and non-uniform spacing [0.459λ, 0.528λ, 0.454λ, 0.421λ, 0.548λ, 0.598λ].

4.2.3 Design of Non-Uniformly Powered and Uniformly Spaced Antenna Array

4.2.3.1 Design of Power Divider

We designed a six-way power divider, shown in **Figure 4.4a**, to realize non-uniform excitation amplitudes of [1, 1, 0.707, 0.707, 0.707, 0.707] in 12 patch elements for SLL reduction. Two one-to-six-way symmetrical power dividers were placed in the opposite direction, and 12 output ports were arranged with a λ/2 distance for uniform spacing. Overall, a 2-to-12 power divider was designed to feed the 12 patch antennas, and two inputs ports were excited with 180° difference to maintain in-phase field excitation in all the antenna elements shown in **Figure 4.4b**. In the one-to-six-way power divider, the input and output transmission lines were designed with 50 Ω characteristic impedance (Z_0), and the quarter wavelength transformers with Z_0 of 35.35 Ω in the junctions 1, 2 and 3 were used to match the impedance between the one input and two output branches of the junction shown in **Figure 4.4a**. Then, the right half of the power divider was mirrored to the left side and a one-to-six power divider design was completed with symmetric form. The spacing between the 12 output ports in Figure 4b was set to λ/2, and the separation between the transformer junctions along the *y* axis was chosen to be greater than half of the guided wavelength for mutual coupling reduction [25]. Overall, ports 8 and 10 receive one-

quarter of the input power, and the other output ports receive the half-power of ports 8 and 10. Therefore, ports 8 and 10 support twice the power of ports 4, 6, 12 and 14.

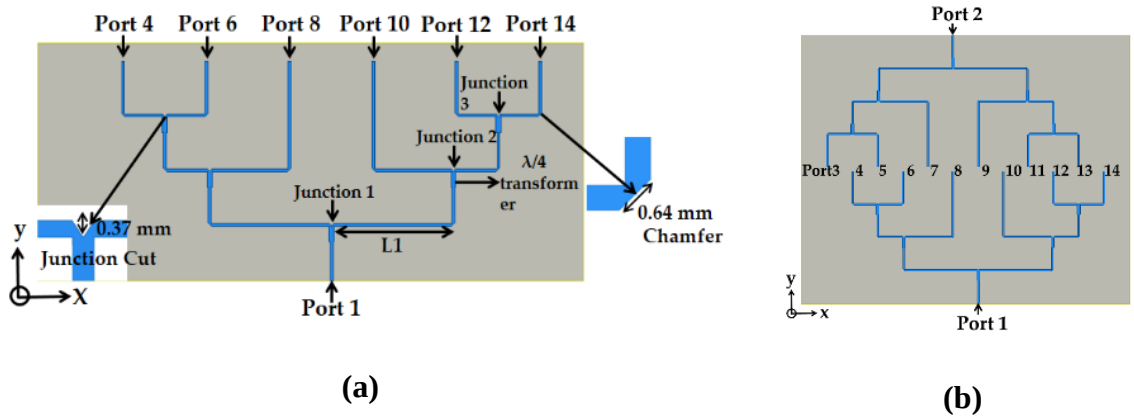

Figure 4.4. (a) one-to-six way non-uniformly powered and uniformly spaced power divider. (b) Two one-to-six-way power dividers for 12 feeding ports to the antenna elements.

Table 2 shows the normalized ideal excitation for ports 4, 6, 8, 10, 12 and 14, which follow the required non-uniform excitation amplitudes of [1, 1, 0.707, 0.707, 0.707, 0.707] for SLL reduction. The simulated power and excitation values from the same ports in the power divider are shown in **Table 4.2**. The simulated values follow the trend as **Table 4.1**, with lower magnitudes due to loss and reflection from the bends and the T-junctions

Table 4.1. Required transmission coefficients, percentages of power, normalized power, and the excitation of the respective ports in the power divider for SLL reduction from Figure 4.4a.

Port	Transmission Coefficient (dB)	Power (%)	Normalized Power	Normalized Excitation
4	−9	12.5	0.5	0.707
6	−9	12.5	0.5	0.707
8	−6	25	1	1
10	−6	25	1	1
12	−9	12.5	0.5	0.707
14	−9	12.5	0.5	0.707

Table 4.2. Simulated transmission coefficients, percentages of power, normalized power, and the excitation of the respective ports in the power divider for SLL reduction from Figure 4.4a.

Port	Transmission Coefficient (dB)	Power (%)	Normalized Power	Normalized Excitation
4	−10.22	9.50	0.454	0.673
6	−10.25	9.44	0.450	0.670
8	−6.79	20.94	1	1
10	−6.80	20.89	0.998	0.998
12	−10.23	9.48	0.452	0.672
14	−10.19	9.57	0.457	0.676

In the power divider design, the reflection from the discontinuities was reduced by chamfering the bending edges and cutting the center of the junction, as shown in **Figure 4. 4a**.

4.2.3.2. Phase Correction of Power Divider

In the designed 2-to-12 power divider, the phase delays for all the output ports should be the same in order to maintain in-phase feeding for all the antenna elements. Because different numbers of quarter-wave impedance transformers were used for different output ports, a modification of the power divider was needed. **Figure 4.5a** shows that the phase delays from port 1 to ports 4, 6, 12 and 14 are the same, at 67°, which is greater than the 42° of the other signal paths for port 8 and 10 at 28 GHz. To balance the phase delays between two different paths, we tuned the length of L1 in the power divider by moving the position of junction 1 and maintaining the positions of the other junctions. We reduced the initial L1 length of 16.37 mm by 0.27 mm in order to compensate for the 25° phase difference. Then, we further tuned L1 in the full-wave simulation, and achieved almost identical phases with an L1 of 16.11 mm, as shown in **Figure 4.5b**. To understand the effect of the output of the optimized power divider on the radiation pattern, we excited the 12 patch elements individually with the realized amplitudes and phases from the power divider, and calculated the normalized gain along theta (θ) in the full-wave simulations. The gain pattern from the array fed by ideal amplitudes and phases was also achieved, and **Figure 4.5c** shows that both patterns are almost overlapped, proving that the designed power divider provides broadside radiation with the desired SLL suppression.

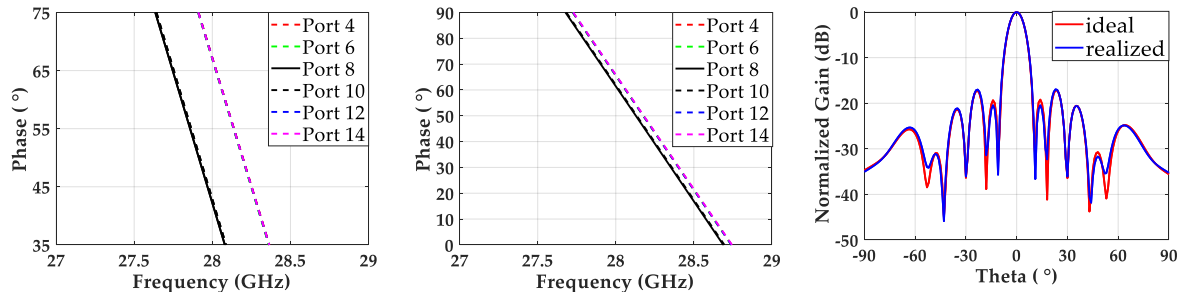

(a) (b) (c)

Figure 4.5. Phase delays from the input port to output ports 4, 6, 8, 10, 12 and 14 when (a) L1 = 16.37 mm and (b) L1 = 16.11 mm. (c) Normalized gain along theta (θ) of the 12 patch elements individually fed by the realized amplitudes and phases from the designed power divider and the ideal values.

4.2.3.3. Patch Integration with Power Divider

We integrated a uniform λ/2-spaced 12-element patch antenna array with the optimized 2-to-12 power divider, as shown in **Figure 4.6a**. On top of the patch antenna elements, the parasitic patches were mounted with a 1 mm air gap, and two input ports (port 1 and port 2) were fed with a 180° phase difference. The simulation results showed a 17.12 dB gain on the boresight, and the normalized radiation pattern in **Figure 4.6b** indicates an SLL of −16.98 dB on the x–z plane. The level of SLL follows the −16.55 dB SLL of the array factor of the corresponding array, indicating that the required non-uniform power distribution was realized through the designed power divider. The nearly 40 dB lower cross-polarized radiation level compared to the co-polarization also indicates that the radiation from the power divider to the cross-polarization is negligible. **Figure 4.6c** shows the wide bandwidth of 9.9% from 26.87 to 29.64 GHz for $S_{11} < -10$ dB.

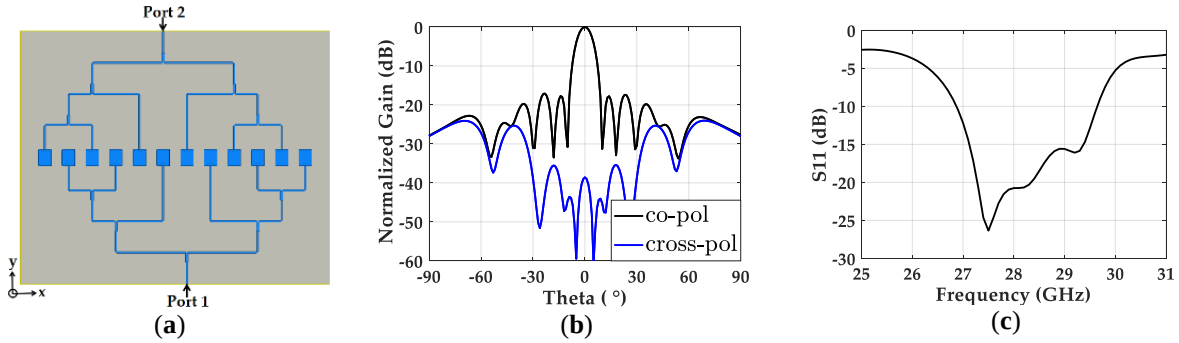

Figure 4.6. (**a**) Top view of the non-uniformly powered and uniformly spaced 12-element patch array. (**b**) Simulated normalized gain of the non-uniformly powered and uniformly spaced 12-element patch array with co- and cross-polarization. (**c**) Simulated S_{11} of the same antenna array.

4.2.4 Design of Non-Uniformly Powered and Non-Uniformly Spaced Antenna Array

To further reduce SLL, we designed a non-uniform inter-element spaced power divider in addition to the non-uniform amplitudes of [1, 1, 0.707, 0.707, 0.707, 0.707]. On top of the non-uniform distances of [0.459λ, 0.528λ, 0.454λ, 0.421λ, 0.548λ, 0.598λ] used in the array factor calculation, we optimized the non-uniform distances using the full-wave simulation to consider the coupling effect of the parasitic patch. The optimum distances for half of the array were [0.498λ, 0.535λ, 0.434λ, 0.418λ, 0.526λ, 0.563λ], and the other side of the array was mirrored, as shown in **Figure 4.7a**. The maximum SLL from the non-uniformly powered 12 patch antennas with the optimized distances without a power divider is nearly −19.25 dB, as shown in **Figure 4.7b**. According to the optimum inter-element spacing for the lowest SLL, we then designed a one-to-six-way power divider and integrated the 12 patch antennas with two sets of one-to-six power dividers.

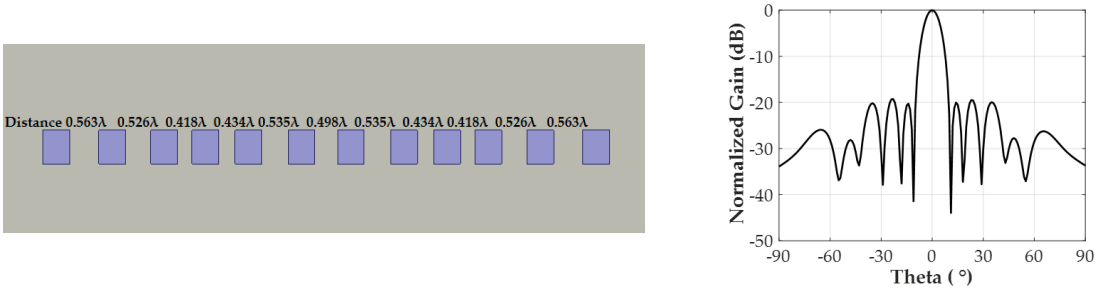

(**a**) (**b**)

Figure 4.7. (**a**) Non-uniformly spaced 12-element patch array without a power divider. (**b**) Normalized gain of the non-uniformly powered and non-uniformly spaced patch array without a power divider in the simulation.

4.2.4.1 Design of Power Divider and Phase Correction

In contrast to the uniformly-spaced power divider, the non-uniformly-spaced structure led to four different signal paths (Port 4 and 6, Port 8, Port 10, and Port 12 and 14) because the power divider lost the symmetry along the *y* axis, as shown in **Figure 4.8a**. In the power divider, L1 can tune phase delays for ports 10, 12 and 14, and L2 can tune only the other signal paths. We changed L1 from 15.7921 mm to 15.575 mm, changed L2 from 16.5152 mm to 16.005 mm, and reduced the phase delay between two different groups with 15° difference, as shown in column 2 of Table 4. However, the tuning of L1 and L2 was not enough to excite all of the ports with identical phase delays.

To further tune the phase delays, we introduced meander lines for ports 10, 12 and 14 in order to tune their physical lengths. Here a, b and c are denoted as the length differences between the straight line and the meander line. The meander lines for ports 12 and 14 increased the paths by 0.38 mm (a = b). The path for port 10 was lengthened by 0.27 mm (c). The added meander lines maintained the maximum phase difference at nearly 5.09°, as shown in column 3 of **Table 4.3**. Finally, we designed a 2-to-12 power divider by mounting a one-to-six power divider rotated along the *y* axis from the opposite side. The 12 output ports of two one-to-six power dividers were arranged with [0.498λ, 0.535λ, 0.434λ, 0.418λ, 0.526λ, 0.563λ] distances, as shown in **Figure 4.8b**. Here, A and A' are symmetric, as are B and B'. Before we connected the power divider to the 12 patch antennas, we excited each antenna with the realized amplitudes and phases from the power divider and calculated the normalized gain along theta (θ). **Figure 4.8c** proves that the gain pattern from the realized output from the power divider is almost the same as the pattern calculated from the array with the ideal in-phase excitation and amplitude tapering.

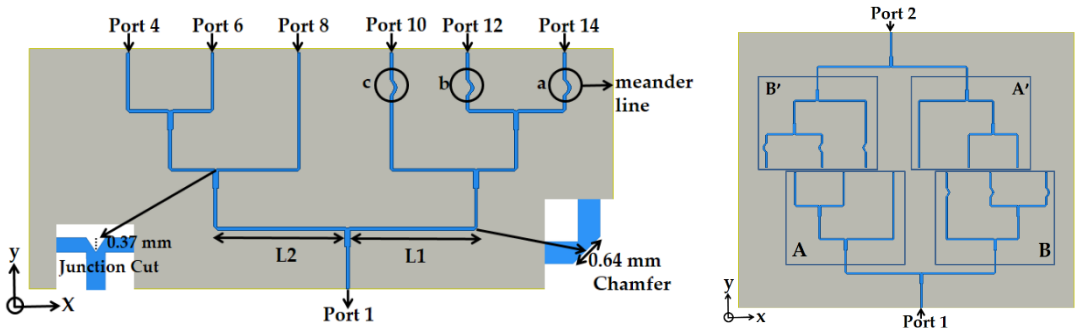

(a) (b)

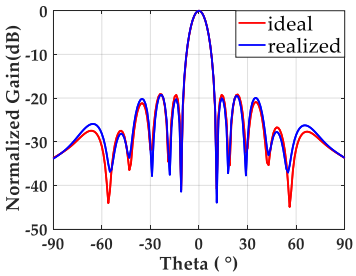

(c)

Figure 4.8. (a) One-to-six-way uniformly powered and spaced power divider. (b) 2-to-12 non-uniformly powered and spaced divider. (c) Normalized gain along theta (θ) of the 12 patch elements individually fed by the realized amplitudes and phases from the designed power divider and the ideal values.

Table 4.3. Phase delays from ports 4, 6, 8, 10, 12 and 14 after tuning L1 and L2, and adding the meander lines in the one-to-six power divider, as shown in Figure 7a.

Port	Phase (Degree) Tuning L1 and L2	Phase (Degree) Tuning L1, L2 and Meander Line
4	87.70	86.18
6	87.58	86.00
8	86.52	85.03
10	98.71	90.12
12	102.11	88.68
14	102.21	89.26

4.2.4.2 Patch Integration with Power Divider

The non-uniformly spaced 2-to-12 power divider was integrated with 12 patch antennas with parasitic elements, as shown in **Figure 4.9a**. Here, two input ports were also fed with a 180° phase difference, and two equal-sized substrates (70 × 57.3 mm^2) for the driven and the parasitic patches were kept at a gap of 1 mm. The radiation pattern from the array on the x–z plane was calculated and is shown in **Figure 4.9b**. It is worth noting that we achieved a nearly 2 dB better SLL (−18.89 dB) with almost the same level of gain (17.05 dB) compared to the antenna array with the uniformly spaced divider. The non-uniformly spaced power divider also maintains low cross-polarized radiation, 32 dB lower than the co-polarization. A similar bandwidth of 9.64%, compared to the uniformly spaced array from 27.05 to 29.75 GHz, was also achieved, as shown in **Figure 4.9c**.

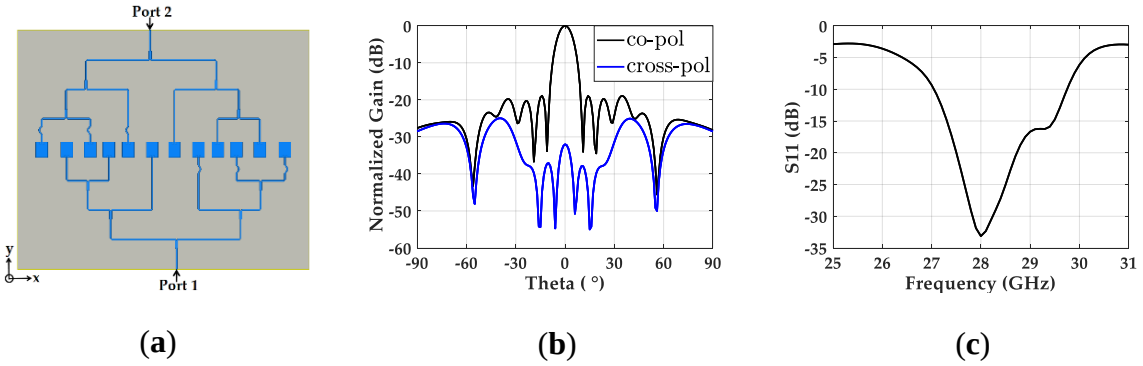

(a) **(b)** **(c)**

Figure 4.9. (a) Top view of the non-uniformly powered and spaced 12-element patch array. (**b**) Simulated normalized gain of the non-uniformly powered and spaced 12-element patch array with co- and cross-polarization. **(c)** Simulated S_{11} of the same antenna array.

4.3. Fabrication and Measurement

For measurement verification, we fabricated the uniformly spaced and the non-uniformly spaced patch antenna arrays in the Rogers 5880 substrate with 70 × 57.3 mm^2, as shown in **Figure 4.10a, b**. Then, the parasitic patches patterned on the same substrate were mounted on top of the array with 1 mm spacing, as depicted in **Figure 4.11a, b**. The 1 mm spacing was maintained with four nylon posts on the corners of the antenna array. We also fabricated a Wilkinson power divider to feed two input ports of the antenna array with a 180° phase shift, and show the top view in **Figure 4.11c**. The Wilkinson divider was chosen due to the high isolation between the output ports. First, we measured the s-parameters from the Wilkinson power divider and confirmed that two signal paths maintained −6 dB and -6.41 dB attenuation, with a phase difference of 184.2° at 28 GHz. Then, we measured S_{11} from the uniformly and the non-uniformly spaced arrays. **Figure 4.12a, b** shows the measured and simulated S_{11} from both arrays, indicating a 15.35% bandwidth (25.16–30.06 GHz) from the uniformly spaced array

and an 11.5% bandwidth (26.24–29.46 GHz) from the non-uniformly spaced array. The measured results showed a wider bandwidth than the simulated ones, by nearly 10%; the discrepancy may come from the stronger coupling between the feeding and the parasitic patches due to the higher parasitic effect in the measurement.

To measure the radiation performance from both antenna arrays, we connected two output ports from the Wilkinson power divider to the two input ports of the antenna array. A horn antenna was used as a transmitting antenna, and a vector network analyzer (Anritsu MS46122B, Anritsu Company, Morgan Hill, USA) was used to measure S_{21} between the horn antenna and the designed antenna arrays fed by the Wilkinson power divider. **Figure 4.13a,b** shows the measuring setup of antenna array. Here the Wilkinson power divider was enclosed by a metallic box to isolate the radiation from the divider and a metallic sheet was placed around the antenna array to minimize further radiation from the divider.

(**a**) (**b**)

Figure 4.10. (**a**) Fabricated non-uniformly powered and uniformly spaced antenna array without parasitic patches. (**b**) Fabricated non-uniformly powered and spaced antenna array without parasitic patches.

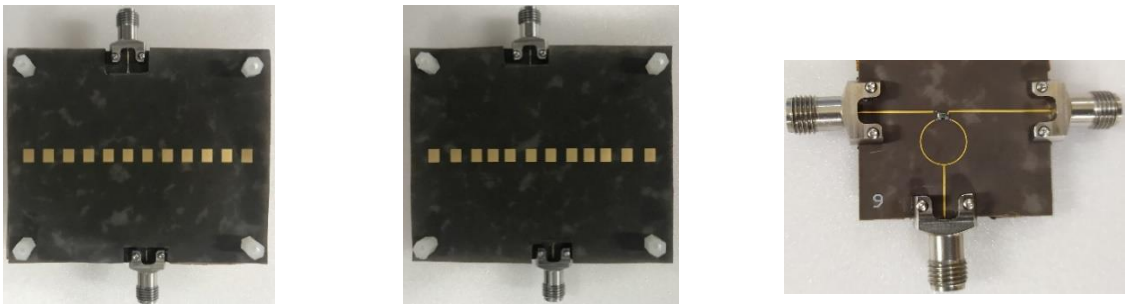

(**a**) (**b**) (**c**)

Figure 4.11. (**a**) Fabricated non-uniformly powered and uniformly spaced antenna array with parasitic patches. (**b**) Fabricated non-uniformly powered and spaced antenna array with parasitic patches. **(c)** Wilkinson power divider for two output ports with 180° phase shift.

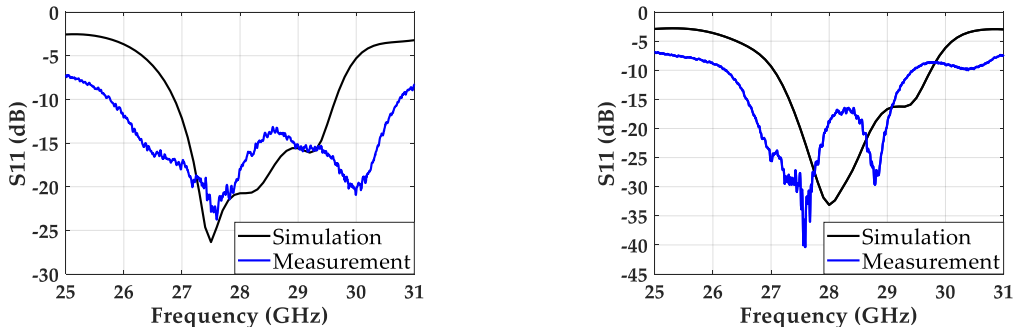

Figure 4.12. Simulation and measured S_{11} of (**a**) the non-uniformly powered and uniformly spaced antenna array, and (**b**) the non-uniformly powered and spaced antenna array.

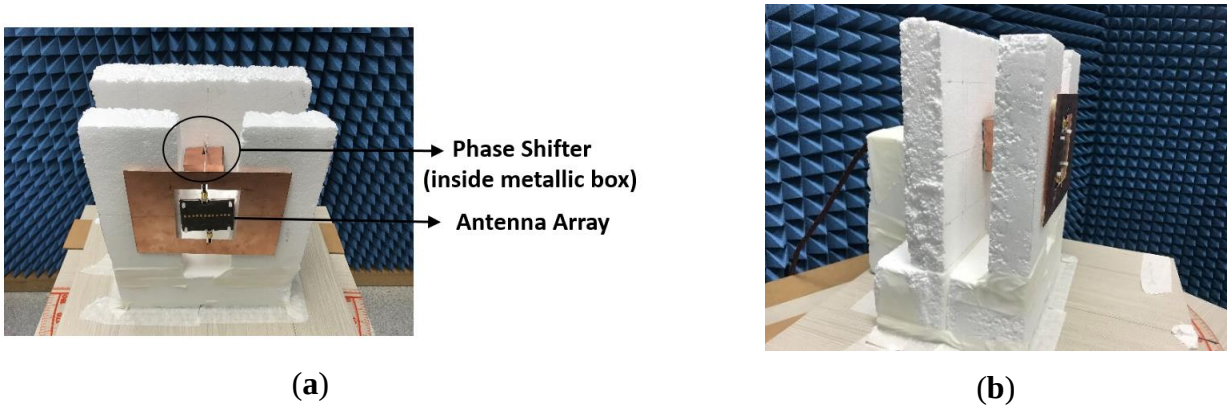

Figure 4.13. Measurement Setup (**a**) Phase shifter with metallic box (**b**) Side view of antenna array and phase shifter

Figure 4.14a shows the measured normalized gain of the non-uniformly powered and uniformly spaced antenna array. The gain of the antenna array was 16.3 dBi at the boresight, and the first side lobe was found as −15.36 dB with an 8° half-power beamwidth. The measured gain and SLL adhere to the levels from the simulation, with differences of nearly 0.8 dB and 1.5 dB, respectively. The normalized gain of the non-uniformly powered and spaced array from **Figure 4.14b** shows a 2 dB lower SLL of −17.27 dB, compared to the uniformly spaced array. This trend follows the simulation results, and experimentally proves the SLL reduction of the non-uniformly spaced patch array operating in the millimeter-wave band. The non-uniformly spaced array also maintained a 16.56 dBi boresight gain and a 7.8° half-power beamwidth, similar to its counterpart.

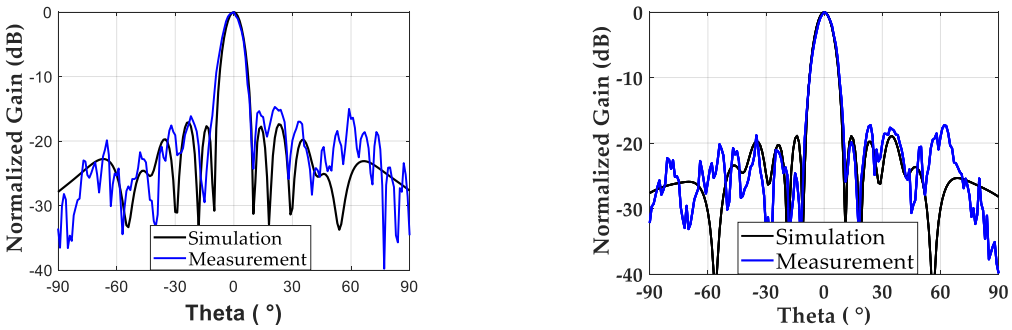

Figure 4.14. Normalized simulation and measurement gain of (**a**) the non-uniformly powered and uniformly spaced antenna array, and (**b**) the non-uniformly powered and spaced antenna array.

4.4 Discussion

The measured gain and SLL from both the uniformly and non-uniformly spaced arrays with the non-uniform excitation followed the levels from the simulation results, with a 1.5 dB difference. The differences between the simulation and measurement results can be attributed to the unequal power levels (−6 dB and −6.41 dB) and the non-ideal phase difference (184.2°) between the two output ports of the fabricated Wilkinson power divider. During the radiation measurement, the Wilkinson power divider was mounted on the backside of the antenna array. Therefore, the current flow on the power divider contributed to the elevated radiations, from 55° to 75°, shown in **Figure 4.13**. The three-port measurement, which can provide two input signals with the desired phase delay, would be a solution to eliminating the undesired radiation from the extra power divider in the antenna input side. We also expect that fabrication inaccuracy, a possible misalignment of the parasitic patches, and mechanical deformation may contribute to the discrepancy between the simulated and the measured results. The last factor could be the diffraction from the surface wave on the finite antenna ground plane [65].

The properties of the reported antenna arrays operating near 28 GHz for 5G applications are summarized in Table 5. We chose the antenna arrays, fed by the microstrip line-based power split network, for a fair comparison. It is worth mentioning that most of the antenna arrays for the 28 GHz band used uniform excitation and spacing, and showed SLL near −13 dB. Only a non-uniformly powered array showed a lower SLL of −15 dB [13]. The proposed microstrip line-based power divider implemented non-uniform inter-element spacing, along with amplitude tapering in the 28 GHz band, for the first time, and demonstrated a superior SLL of −17 dB with the 12-patch antenna array. This SLL is nearly 4 dB lower than the reported −13.4 dB SLL from the parasitic patch-integrated uniformly spaced antenna array [56].

Table 4.4. Performance comparison of the antenna arrays, fed by the microstrip-based power divider, operating near 28 GHz for 5G applications.

Ref#	**Power Dist.**	**Element Spacing**	**Element No#**	**fo (GHz)**	**Gain (dBi)**	**SLL** [1] **(dB)**	**Impedance Bandwidth**	**Radiation Efficiency**	**Half Power Beam Width**
[58]	uniform	uniform	4	28	16.3	−11.6	17.85%	71.8%	11°
[66]	uniform	uniform	8	28	13	~	21.4%	75%	~
[67]	uniform	uniform	8	28	11.32	~	14.1%	~	~
[57]	uniform	uniform	8	28	12	−12.5	17.87%	>65%	12.5°
[59]	non-uniform	uniform	8	26	12	−15	21.15%	>90%	13.3°
[56]	uniform	uniform	16	28	19.66	−13.4	24.4%	86%	5°
This work	non-uniform	uniform	12	28	16.3	−15.4	15.35%	~80%	8.84°
	non-uniform	non-uniform	12	28	16.56	−17.3	11.5%	~80%	8.9°

[1] Sidelode level (SLL).

CHAPTER 5: CONCLUSIONS AND FUTURE WORKS

5.1 Conclusions

In this paper, we designed a non-uniformly excited and spaced power divider using the microstrip line to feed a 12-element patch antenna array with parasitic patches for high gain and low SLL at 28 GHz. For higher isolation between adjacent patch antenna elements, including parasitic patches, two signals of input into the power divider with 180° difference were utilized. The fabricated non-uniformly powered and spaced antenna array, integrated with the designed power divider, demonstrated a 16.56 dBi boresight gain and a low SLL of −17.27 dB at 28 GHz. As a counterpart, we also designed a non-uniformly powered but uniformly spaced power divider and the integrated structure with the 12-element patch array showed a higher SLL of −15.3 dB in the measurement. This comparison effectively proved SLL reduction as a result of the non-uniform inter-element spacing. Both antenna arrays also showed a wide bandwidth of more than 10% due to coupling with parasitic patches. Finally, we expect that the non-uniformly powered and spaced high-gain patch antenna array, with a low SLL in the fabrication-friendly microstrip line, can be utilized for a high-gain beam-forming system in millimeter-wave communication.

5.2 Suggestion for Future Work

In the future, we can expand our research for multiple beam forming for 5G applications by both uniform and non-uniform spacing of the array. This beam forming can be realized by providing phase difference to the corresponding antenna elements. Most importantly, it is necessary to maintain the gain deviation lower than 3dB while beam scanning in a specific direction. Meanwhile, an aperture feeding technique can be implemented to hide the feed line to achieve more SLL reduction on the specified frequency regime. However, the beam forming criteria for uniform and non-uniform distance array has discussed as following.

5.2.1 Uniform Spaced Array Beam forming

For beam scanning realization we can rewrite the Equation-20 and can identify the scanning angle.

$$\mathrm{AF}(\theta) = \sum_{n=-6}^{6} a_n e^{j(kx_n \sin(\theta) - kx_n \sin(\theta_0))} \tag{21}$$

Apart from Equation-20 a new term $kx_n \sin(\theta_0)$ has appeared in the Equation-21. This is the definite

phase difference between the adjacent antenna elements and θ_0 is the scanning angle. By putting the value of θ_0 we can identify the corresponding phases of nth elements of the antenna. In figure 5.1, twelve elements of the array with uniform half-wavelength spacing without power divider has shown. The corresponding antenna elements can be feed with non-uniform excitation and phases for beam scanning realization. According to the calculation from the definite phase difference, we can realize the beam scanning by HFSS simulation from -50° to +50°, which are shown in Figures 5.2 to 5.6. The SLL increases from -16.7 to -14.19 dB within this scanning range. This SLL at ±50° is within the 3dB SLL difference from broadside direction (-17.04 dB). So this array is compatible with a 100° scanning range.

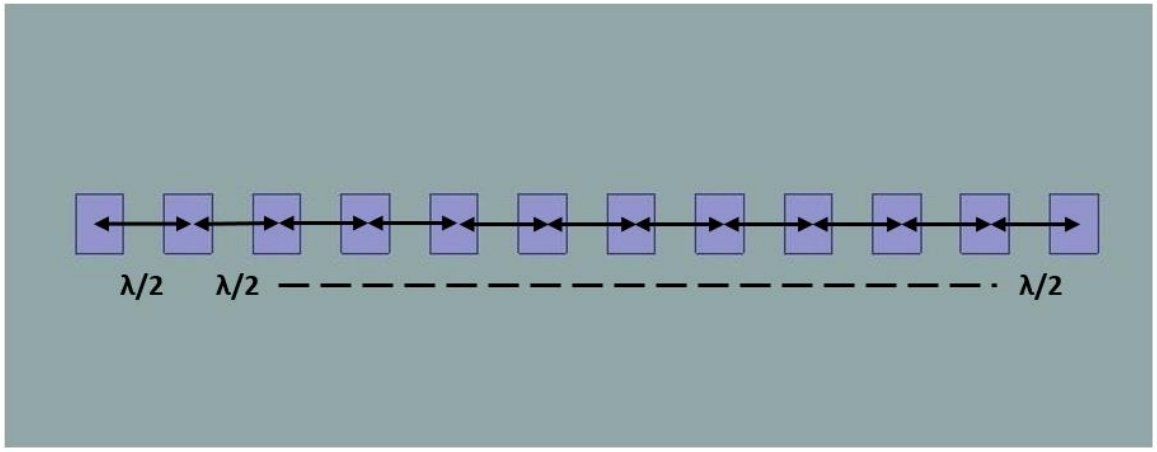

Figure 5.1. Uniform half-wavelength spaced array without power divider

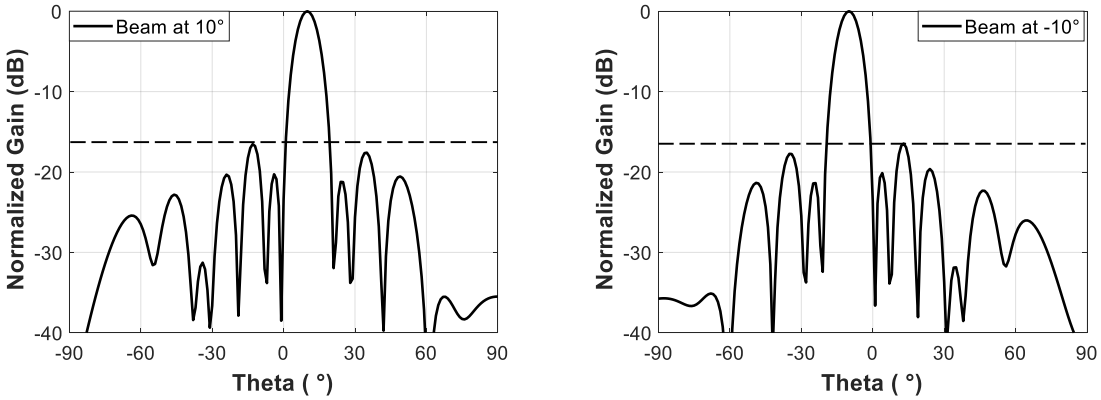

(**a**) (**b**)

Figure 5.2. Simulation of uniform spaced array without power divider (SLL= -16.77) (**a**) 10° (**b**) -10°

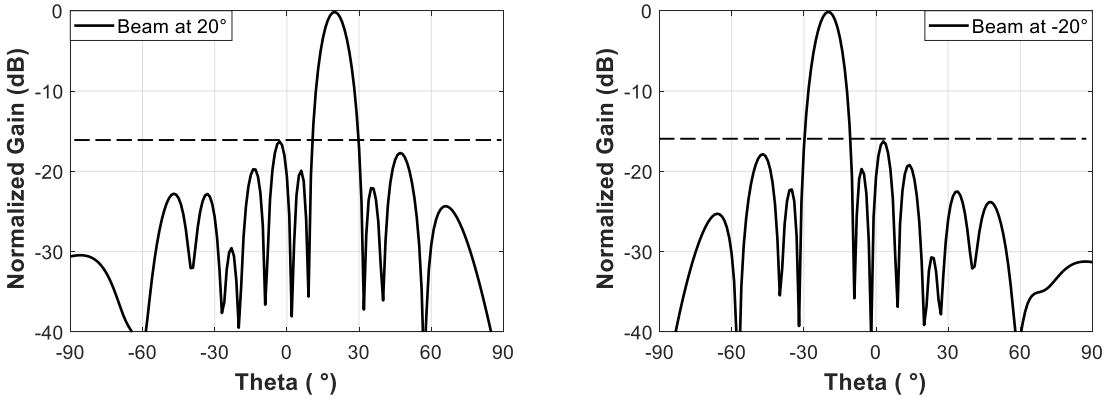

(**a**) (**b**)

Figure 5.3. Simulation of uniform spaced array without power divider (SLL= -16.13) (**a**) 20° (**b**) -20°

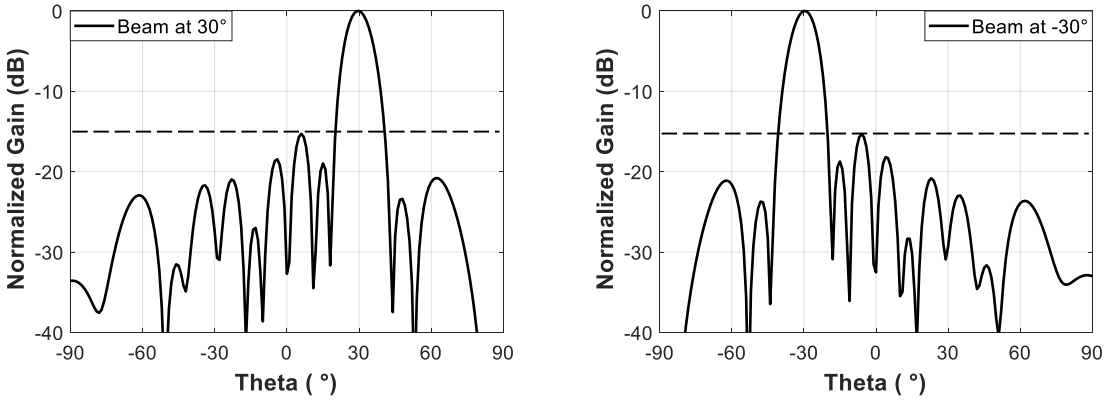

(**a**) (**b**)

Figure 5.4. Simulation of uniform spaced array without power divider (SLL= -15.27) (**a**) 30° (**b**) -30°

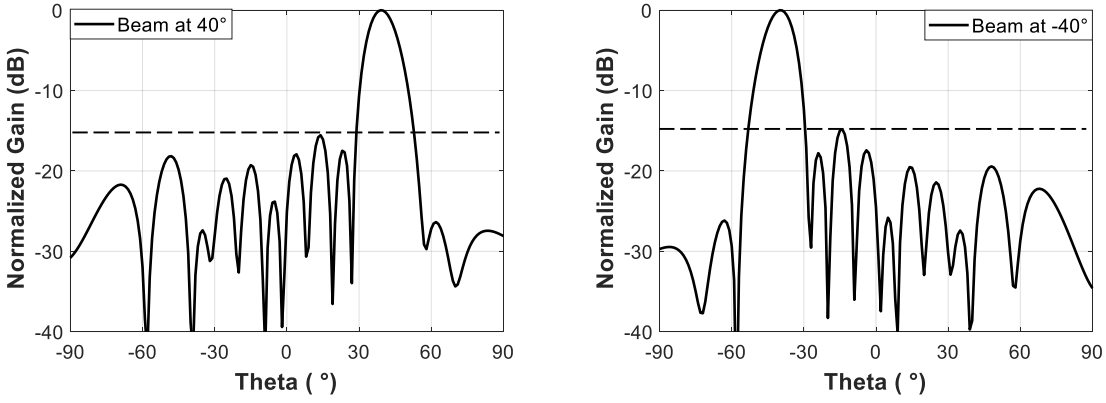

(**a**) (**b**)

Figure 5.5. Simulation of uniform spaced array without power divider (SLL= -15.5) (**a**) 40° (**b**) -40°

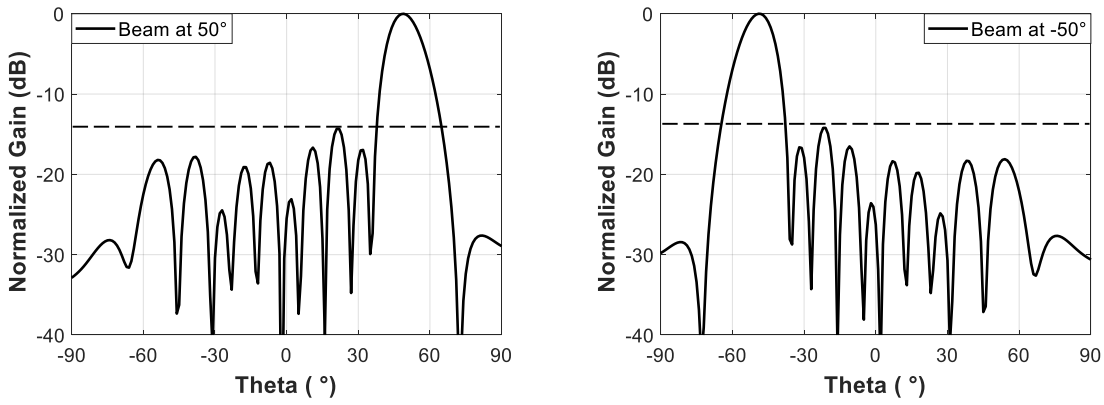

(**a**) (**b**)

Figure 5.6. Simulation of uniform spaced array without power divider (SLL= -14.13) (**a**) 50° (**b**) -50°

5.2.2 Non-Uniform Spaced Array Beam forming

According to the same procedure we followed in the previous section we can identify the scanning angle and feed the antenna elements with corresponding power and phases for scanning the non-uniformly spaced array. Figure 5.7, represents the non-uniform spaced array without power divider realization. Following the calculation from the definite phase difference, we can realize the beam scanning by HFSS simulation from -50° to +50°, which are shown in Figures 5.8 to 5.12. The SLL increases from -18.93 to -11.52 dB within the scanning range. At ±50°, the SLL is -11.52 dB which is very high compared to SLL when the beam is directed to broadside (0°). But at ±40° the SLL is -16.6 dB which is in the 3dB side lobe level compared to the broadside SLL. So this array is compatible with the 80° (-40° to +40°) scanning range.

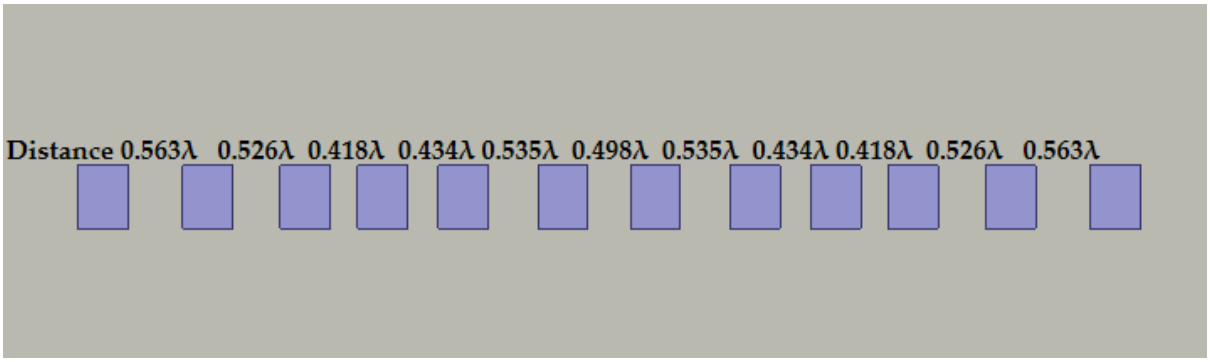

Figure 5.7. Non-uniform spaced array without power divider

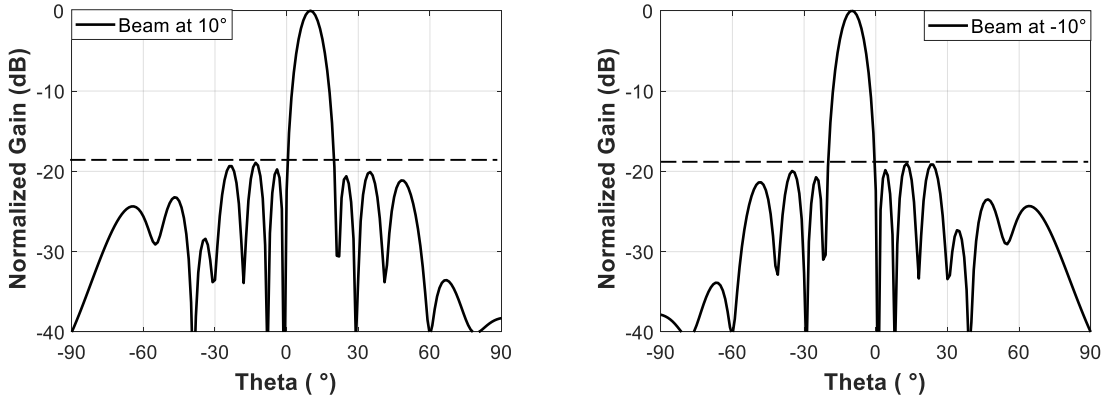

(**a**) (**b**)

Figure 5.8. Simulation of non-uniform spaced array without divider (SLL= -18.93) (**a**) 10° (**b**) -10°

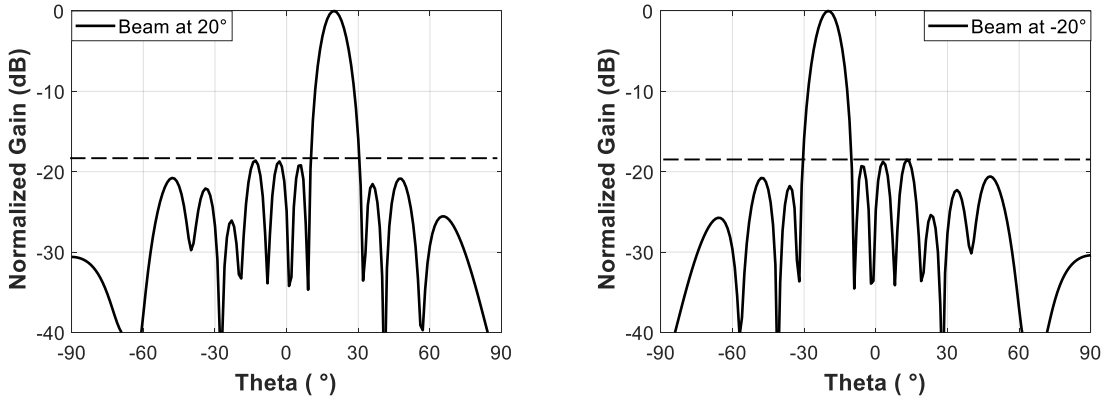

(**a**) (**b**)

Figure 5.9. Simulation of non-uniform spaced array without divider (SLL= -18.60) (**a**) 20° (**b**) -20°

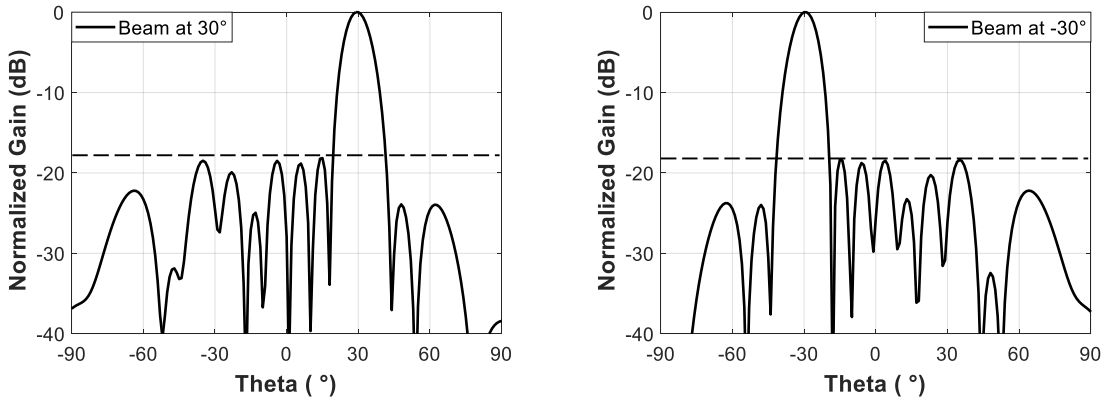

(**a**) (**b**)

Figure 5.10. Simulation of non-uniform spaced array without divider (SLL= -18.15) (**a**) 30° (**b**) -30°

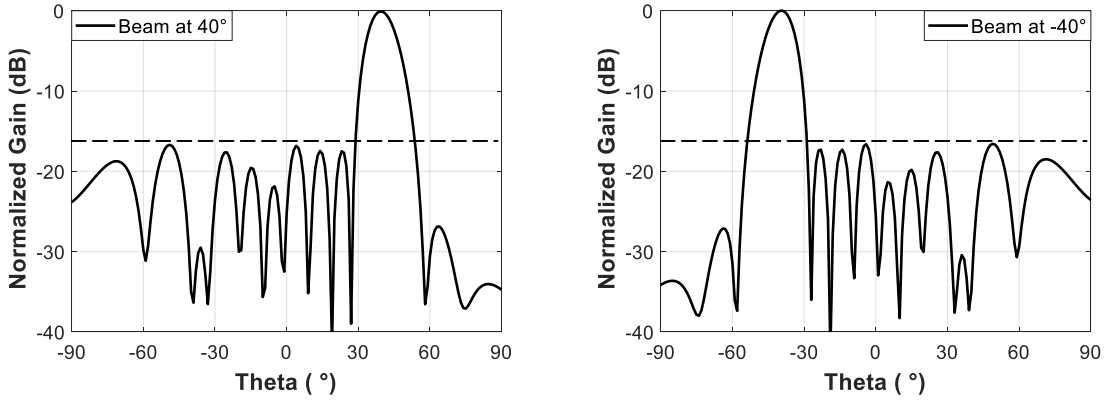

(**a**) (**b**)

Figure 5.11. Simulation of non-uniform spaced array without divider (SLL= -16.62) (**a**) 40° (**b**) -40°

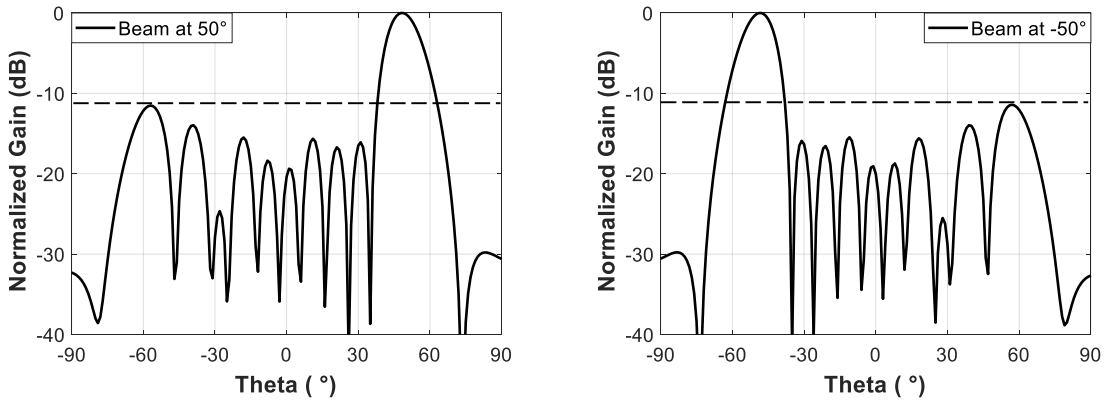

(**a**) (**b**)

Figure 5.12. Simulation of non-uniform spaced array without divider (SLL= -11.42) (**a**) 50° (**b**) -50°

5.2.3 Discussion About Beam-forming Array

The uniform spaced array can be used to scan the beam from +50° to -50° where the non-uniform spaced array can scan +40° to -40°. It's because of the mutual coupling between the antenna elements. Uniform spaced arrays are uniform λ/2 spaced arrays as shown in Figure 5.1. On the other hand, the non-uniform spaced array has some spacing which is lower than λ/2 (0.418λ and 0.434λ) as shown in Figure 5.7. In that case, mutual coupling between the antenna elements will not be similar to a uniform array. Therefore, while steering the beam of a non-uniform spaced array near 50°, the mutual coupling between the elements may create an interference due to the field interference from the adjacent elements and hence radiation pattern can be changed. Thus, the SLL of the non-uniform array will be high near 50°. To validate this condition we plotted the E field distribution on an x-z plane for uniform and non-uniform cases which have shown in Figures 5.13 and 5.14. Here, the E field is directed and bent to the direction of interest for both cases and it has higher mutual interception for non-uniform array compared to the uniform array. To minimize the mutual coupling we can introduce a meander line

between the adjacent antenna elements in our future work [68]. Although this discussion is only limited to the beam forming array without a power divider, in the future our work will cover the array with a power divider to realize the definite phase difference among the antenna elements by phase-shifting topology.

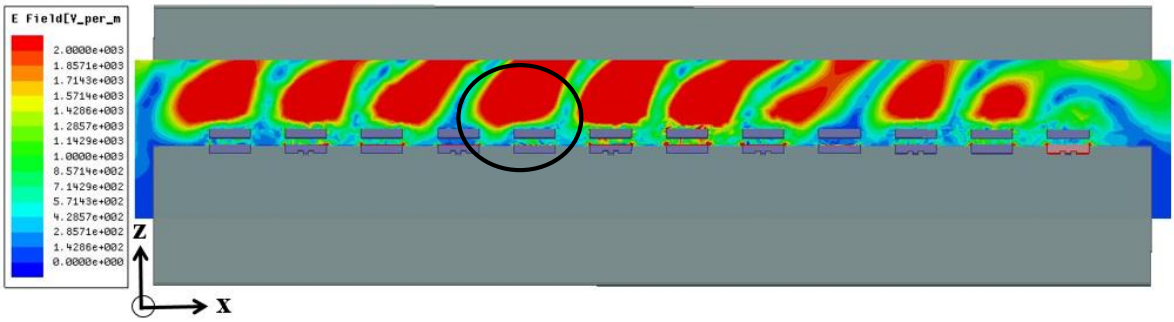

Figure 5.13. E Field at +50° for uniform array (circle represent low interception of E field)

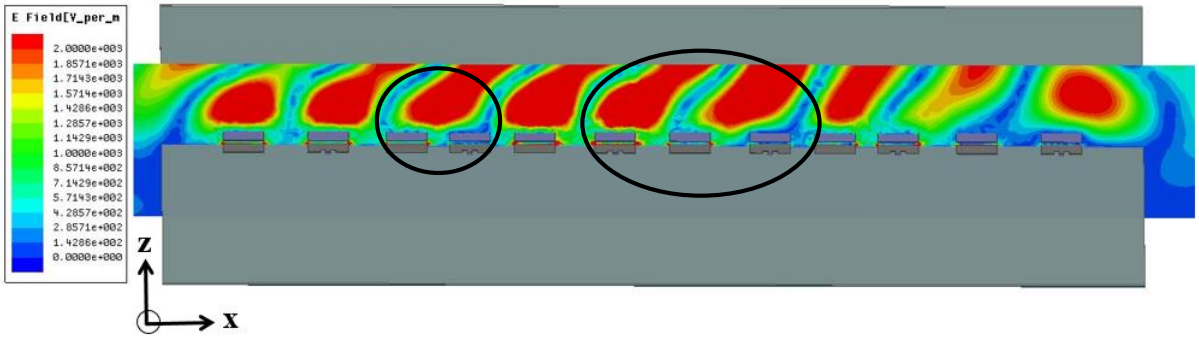

Figure 5.14. E Field at +50° for non-uniform array (circle represent high interception of E field)

References:

[1] C. A. Balanis, *Antenna theory: analysis and design*. John wiley & sons, 2016.

[2] S. Ogurtsov and S. Koziel, "Systematic approach to sidelobe reduction in linear antenna arrays through corporate-feed-controlled excitation," *IET Microwaves, Antennas & Propagation*, vol. 11, no. 6, pp. 779–786, 2016.

[3] G. A. Deschamps, "Microstrip microwave antennas," in *Proceedings of the Third Symposium on the USAF Antenna Research and Development Program, Oct*, 1953, pp. 18–22.

[4] H. Gutton and G. Baissinot, "Flat aerial for ultra high frequencies," *French patent*, vol. 703113, 1955.

[5] J. Q. Howell, "Microstrip antennas," *ITAP*, vol. 23, pp. 90–93, 1975.

[6] R. Garg, P. Bhartia, I. J. Bahl, and A. Ittipiboon, *Microstrip antenna design handbook*. Artech house, 2001.

[7] M. Kara, "Formulas for the computation of the physical properties of rectangular microstrip antenna elements with various substrate thicknesses," *Microwave and Optical Technology Letters*, vol. 12, no. 4, pp. 234–239, 1996.

[8] C. Krowne, "Cylindrical-rectangular microstrip antenna," *IEEE Transactions on Antennas and Propagation*, vol. 31, no. 1, pp. 194–199, 1983.

[9] Y. Qian, R. Coccioli, D. Sievenpiper, V. Radisic, E. Yablonovitch, and T. Itoh, "A microstrip patch antenna using novel photonic band-gap structures," *Microwave Journal*, vol. 42, no. 1, pp. 66–72, 1999.

[10] G. Kumar and K. Gupta, "Nonradiating edges and four edges gap-coupled multiple resonator broad-band microstrip antennas," *IEEE Transactions on antennas and propagation*, vol. 33, no. 2, pp. 173–178, 1985.

[11] C. Wood, "Improved bandwidth of microstrip antennas using parasitic elements," in *IEE Proceedings H (Microwaves, Optics and Antennas)*, 1980, vol. 127, no. 4, pp. 231–234.

[12] E. Nishiyama and M. Aikawa, "Wide-band and high-gain microstrip antenna with thick parasitic patch substrate," in *IEEE Antennas and Propagation Society Symposium, 2004.*, 2004, vol. 1, pp. 273–276.

[13] H. Oltman and D. Huebner, "Electromagnetically coupled microstrip dipoles," *IEEE Transactions on Antennas and Propagation*, vol. 29, no. 1, pp. 151–157, 1981.

[14]A. Sabban, "A new broadband stacked two-layer microstrip antenna," in *1983 Antennas and Propagation Society International Symposium*, 1983, vol. 21, pp. 63–66

[15] C. Chen, A. Tulintseff, and R. Sorbello, "Broadband two-layer microstrip antenna," in *1984 Antennas and Propagation Society International Symposium*, 1984, vol. 22, pp. 251–254.

[16] P. S. Bhatnagar, J.-P. Daniel, K. Mahdjoubi, and C. Terret, "Experimental study on stacked triangular microstrip antennas," *Electronics Letters*, vol. 22, no. 16, pp. 864–865, 1986.

[17] R. Q. Lee and K. F. Lee, "Gain enhancement of microstrip antennas with overlaying parasitic directors," *Electronics Letters*, vol. 24, no. 11, pp. 656–658, 1988.

[18] R. Q. Lee, K. F. Lee, and J. Bobinchak, “Characteristics of a two-layer electromagnetically coupled rectangular patch antenna,” *Electronics letters*, vol. 23, no. 20, pp. 1070–1072, 1987.

[19] R. Q. Lee and K. F. Lee, “Effects of parasitic patch sizes on multi-layer electromagnetically coupled patch antenna,” in *Digest on Antennas and Propagation Society International Symposium*, 1989, pp. 624–627.

[20] S. Egashira and E. Nishiyama, “Stacked microstrip antenna with wide bandwidth and high gain,” *IEEE Transactions on Antennas and Propagation*, vol. 44, no. 11, pp. 1533–1534, 1996.

[21] J. Anguera, G. Font, C. Puente, C. Borja, and J. Soler, “Multifrequency microstrip patch antenna using multiple stacked elements,” *IEEE microwave and wireless components letters*, vol. 13, no. 3, pp. 123–124, 2003.

[22] E. Nishiyama and M. Aikawa, “Wide-band and high-gain microstrip antenna with thick parasitic patch substrate,” in *IEEE Antennas and Propagation Society Symposium, 2004.*, 2004, vol. 1, pp. 273–276.

[23] R. Munson, “Microstrip phased array antennas,” in *1973 EIC 11th Electrical Insulation Conference*, 1973, pp. 281–283.

[24] R. Munson, “Conformal microstrip antennas and microstrip phased arrays,” *IEEE Transactions on Antennas and propagation*, vol. 22, no. 1, pp. 74–78, 1974.

[25] T.-S. Horng and N. G. Alexopoulos, “Corporate feed design for microstrip arrays,” *IEEE Transactions on Antennas and Propagation*, vol. 41, no. 12, pp. 1615–1624, 1993.

[26] “Antennas and Phased Arrays,” *RF Microtech*. https://rfmicrotech.com/products-smart-solutions/antennas-and-phased-arrays/ (accessed Oct. 22, 2020).

[27] J. S. Stone, United States Patent no. 1,643,323 and No. 1,715,433

[28] C.L. Dolph, "A Current Distribution for Broadside Arrays Which Optimizes the Relationship Between Beam Width and Side-Lobe Level," IRE Proc., vol. 34, June 1946, pp. 335-348

[29] R. J. Stegen, “Excitation coefficients and beamwidths of Tschebyscheff arrays,” *Proceedings of the IRE*, vol. 41, no. 11, pp. 1671–1674, 1953.

[30] D. Barbiere, “A method for calculating the current distribution of Tschebyscheff arrays,” *Proceedings of the IRE*, vol. 40, no. 1, pp. 78–82, 1952.

[31] R. Chopra and G. Kumar, “Series-fed binomial microstrip arrays for extremely low sidelobe level,” *IEEE Transactions on Antennas and Propagation*, vol. 67, no. 6, pp. 4275–4279, 2019.

[32] J. Liu, D. R. Jackson, Y. Li, C. Zhang, and Y. Long, “Investigations of SIW leaky-wave antenna for endfire-radiation with narrow beam and sidelobe suppression,” *IEEE Transactions on antennas and Propagation*, vol. 62, no. 9, pp. 4489–4497, 2014.

[33] B. Singh, N. Sarwade, and K. P. Ray, “Non-identical rectangular microstrip antenna arrays for amplitude tapering,” *IETE Journal of research*, vol. 64, no. 3, pp. 387–393, 2018.

[34] B. Singh, N. Sarwade, and K. P. Ray, “Uniformly tapered linear array using non identical rectangular microstrip antenna elements,” in *2017 IEEE Applied Electromagnetics Conference (AEMC)*, 2017, pp. 1–2.

[35] Z. Chen and S. Otto, “A taper optimization for pattern synthesis of microstrip series-fed patch array antennas,” in *2009 European Wireless Technology Conference*, 2009, pp. 160–163.

[36] R. Bayderkhani and H. R. Hassani, “Wideband and low sidelobe slot antenna fed by series-fed printed array,” *IEEE Transactions on Antennas and Propagation*, vol. 58, no. 12, pp. 3898–3904, 2010.

[37] D.-F. Guan, C. Ding, Z.-P. Qian, Y.-S. Zhang, W.-Q. Cao, and E. Dutkiewicz, “An SIW-based large-scale corporate-feed array antenna,” *IEEE transactions on antennas and propagation*, vol. 63, no. 7, pp. 2969–2976, 2015.

[38] S.-J. Park, D.-H. Shin, and S.-O. Park, “Low side-lobe substrate-integrated-waveguide antenna array using broadband unequal feeding network for millimeter-wave handset device,” *IEEE Transactions on Antennas and Propagation*, vol. 64, no. 3, pp. 923–932, 2015.

[39] L. Chang, Y. Li, Z. Zhang, X. Li, S. Wang, and Z. Feng, “Low-sidelobe air-filled slot array fabricated using silicon micromachining technology for millimeter-wave application,” *IEEE Transactions on Antennas and Propagation*, vol. 65, no. 8, pp. 4067–4074, 2017.

[40] T. Potelon, M. Ettorre, and R. Sauleau, “Long Slot Array Fed by a Nonuniform Corporate Feed Network in PPW Technology,” *IEEE Transactions on Antennas and Propagation*, vol. 67, no. 8, pp. 5436–5445, 2019.

[41] Y. J. Cheng, J. Wang, and X. L. Liu, “94 GHz substrate integrated waveguide dual-circular-polarization shared-aperture parallel-plate long-slot array antenna with low sidelobe level,” *IEEE Transactions on Antennas and Propagation*, vol. 65, no. 11, pp. 5855–5861, 2017.

[42] J.-W. Lian, Y.-L. Ban, J.-Q. Zhu, J. Guo, and Z. Chen, “Planar 2-D scanning SIW multibeam array with low sidelobe level for millimeter-wave applications,” *IEEE Transactions on Antennas and Propagation*, vol. 67, no. 7, pp. 4570–4578, 2019.

[43] S. Ogurtsov and S. Koziel, “On alternative approaches to design of corporate feeds for low-sidelobe

microstrip linear arrays," *IEEE Transactions on Antennas and Propagation*, vol. 66, no. 7, pp. 3781–3786, 2018.

[44] J. Yin, Q. Wu, C. Yu, H. Wang, and W. Hong, "Low-sidelobe-level series-fed microstrip antenna array of unequal interelement spacing," *IEEE Antennas and Wireless Propagation Letters*, vol. 16, pp. 1695–1698, 2017.

[45] H. Yi, L. Li, J. Han, and Y. Shi, "Traveling-Wave Series-Fed Patch Array Antenna Using Novel Reflection-Canceling Elements for Flexible Beam," *IEEE Access*, vol. 7, pp. 111466–111476, 2019.

[46] A. Sharaqa and N. Dib, "Position-only side lobe reduction of a uniformly excited elliptical antenna array using evolutionary algorithms," *IET Microwaves, Antennas & Propagation*, vol. 7, no. 6, pp. 452–457, 2013.

[47] T. S. Rappaport *et al.*, "Millimeter wave mobile communications for 5G cellular: It will work!," *IEEE access*, vol. 1, pp. 335–349, 2013.

[48] Z. Pi and F. Khan, "An introduction to millimeter-wave mobile broadband systems," *IEEE communications magazine*, vol. 49, no. 6, pp. 101–107, 2011.

[49] T. Bai and R. W. Heath, "Coverage and rate analysis for millimeter-wave cellular networks," *IEEE Transactions on Wireless Communications*, vol. 14, no. 2, pp. 1100–1114, 2014.

[50] W. Hong, K.-H. Baek, Y. Lee, Y. Kim, and S.-T. Ko, "Study and prototyping of practically large-scale mmWave antenna systems for 5G cellular devices," *IEEE Communications Magazine*, vol. 52, no. 9, pp. 63–69, 2014.

[51] A. V. Alejos, M. G. Sanchez, and Iñ. Cuinas, "Measurement and analysis of propagation mechanisms at 40 GHz: Viability of site shielding forced by obstacles," *IEEE Transactions on Vehicular Technology*, vol. 57, no. 6, pp. 3369–3380, 2008.

[52] S. Zhang, X. Chen, I. Syrytsin, and G. F. Pedersen, "A planar switchable 3-D-coverage phased array antenna and its user effects for 28-GHz mobile terminal applications," *IEEE Transactions on Antennas and Propagation*, vol. 65, no. 12, pp. 6413–6421, 2017.

[53] P. A. Dzagbletey and Y.-B. Jung, "Stacked microstrip linear array for millimeter-wave 5G baseband communication," *IEEE Antennas and Wireless Propagation Letters*, vol. 17, no. 5, pp. 780–783, 2018.

[54] T. Seki, N. Honma, K. Nishikawa, and K. Tsunekawa, "Millimeter-wave high-efficiency multilayer parasitic microstrip antenna array on teflon substrate," *IEEE Transactions on Microwave Theory and Techniques*, vol. 53, no. 6, pp. 2101–2106, 2005.

[55] M. Akbari, M. Farahani, A. R. Sebak, and T. A. Denidni, "A 30ghz high-gain circularly-polarized pattem-steerable antenna based on parasitic patches," in *2017 11th European Conference on Antennas and Propagation*

(EUCAP), 2017, pp. 3044–3046.

[56] M. Khalily, R. Tafazolli, P. Xiao, and A. A. Kishk, "Broadband mm-wave microstrip array antenna with improved radiation characteristics for different 5G applications," *IEEE Transactions on Antennas and Propagation*, vol. 66, no. 9, pp. 4641–4647, 2018.

[57] S. Chen and A. Zhao, "Wideband 28 GHz ground reflected dipole antenna and array for 5G mobile handset," in *2018 IEEE International Symposium on Antennas and Propagation & USNC/URSI National Radio Science Meeting*, 2018, pp. 243–244.

[58] O. M. Haraz, A. Elboushi, S. A. Alshebeili, and A.-R. Sebak, "Dense dielectric patch array antenna with improved radiation characteristics using EBG ground structure and dielectric superstrate for future 5G cellular networks," *IEEE Access*, vol. 2, pp. 909–913, 2014.

[59] C.-X. Mao, M. Khalily, P. Xiao, T. W. Brown, and S. Gao, "Planar sub-millimeter-wave array antenna with enhanced gain and reduced sidelobes for 5G broadcast applications," *IEEE Transactions on Antennas and Propagation*, vol. 67, no. 1, pp. 160–168, 2018.

[60] Q. You, Y. Lu, Y. You, Y. Wang, Z.-C. Hao, and J. Huang, "Wideband full-corporate-feed waveguide continuous transverse stub antenna array," *IEEE Access*, vol. 6, pp. 76673–76681, 2018.

[61] E. García-Marín, J. L. Masa-Campos, P. Sánchez-Olivares, and J. A. Ruiz-Cruz, "Evaluation of Additive Manufacturing Techniques Applied to Ku-Band Multilayer Corporate Waveguide Antennas," *IEEE Antennas and Wireless Propagation Letters*, vol. 17, no. 11, pp. 2114–2118, Nov. 2018, doi: 10.1109/LAWP.2018.2866631.

[62] S. Ogurtsov and S. Koziel, "Systematic approach to sidelobe reduction in linear antenna arrays through corporate-feed-controlled excitation," *IET Microwaves, Antennas & Propagation*, vol. 11, no. 6, pp. 779–786, 2016.

[63] H. Legay and L. Shafai, "New stacked microstrip antenna with large bandwidth and high gain," *IEE Proceedings-Microwaves, Antennas and Propagation*, vol. 141, no. 3, pp. 199–204, 1994.

[64]"Ansys HFSS: High Frequency Electromagnetic Field Simulation Software." https://www.ansys.com/products/electronics/ansys-hfss (accessed Oct. 23, 2020).

[65] D. M. Pozar and B. Kaufman, "Design considerations for low sidelobe microstrip arrays," *IEEE Transactions on Antennas and Propagation*, vol. 38, no. 8, pp. 1176–1185, 1990.

[66] M. Stanley, Y. Huang, T. Loh, Q. Xu, H. Wang, and H. Zhou, "A high gain steerable millimeter-wave antenna array for 5G smartphone applications," in *2017 11th European Conference on Antennas and Propagation*

(EUCAP), 2017, pp. 1311–1314.

[67] S. Zhu, H. Liu, Z. Chen, and P. Wen, "A compact gain-enhanced Vivaldi antenna array with suppressed mutual coupling for 5G mmWave application," *IEEE Antennas and Wireless Propagation Letters*, vol. 17, no. 5, pp. 776–779, 2018.

[68] S. R. Govindarajulu, A. Jenkel, R. Hokayem, and E. A. Alwan, "Mutual coupling suppression in antenna arrays using meandered open stub filtering technique," IEEE Open Journal of Antennas and Propagation, vol. 1, pp. 379–386, 2020.